Title
Performance of Conductive Polymers as Binders for Lithium-Ion Batteries

Author
Zhai, Kuan

Publication Date
2022

Peer reviewed|Thesis/dissertation

UNIVERSITY OF CALIFORNIA

Los Angeles

Performance of Conductive Polymers as Binders for Lithium-Ion Batteries

A dissertation submitted in partial satisfaction of the requirements for the degree Master of Science in Materials Science and Engineering

by

Kuan Zhai

2022

ABSTRACT OF THE THESIS

Performance of Conductive Polymers

as Binders for Lithium-Ion Batteries

by

Kuan Zhai

Master of Science in Materials Science and Engineering

University of California, Los Angeles, 2022

Professor Bruce Dunn, Chair

The growing market for energy storage devices raises the demand for lithium ion batteries (LIBs) with higher energy density and power density. Enhanced LIB performance requires the improvement of the electrode materials, so that the use of conductive polymer binders becomes an important option when the choice of active materials is limited. Compared to a traditional binder, such as PVDF, the advanced polymer binders exhibit not only electrochemical stability and adhesion strength, but also ionic/electronic conductivity for a thick electrode and/or a high-capacity electrode. Such considerations make the 3,4-propylenedioxythiophene-2,5-dicarboxylic acid family (ProDOT) and poly{[N,N′-bis(2-octyldodecyl)-naphthalene-1,4,5,8-

bis (dicarboximide)-2,6-diyl]-alt-5,5 ′ -(2,2 ′ -bithiophene)} family (P(NDI2OD-T2)) of polymers attractive candidates for the LIB binders.

Various experiments were designed and conducted on the selected binder candidates in order to evaluate different aspects of polymer behavior. The material properties are investigated based on thin film three-electrode systems, while the half-cell and full-cell experiments represent how the binder influences the electrodes and practical batteries, respectively. According to those experiments, the Hexyl-ProDOT polymer shows excellent mixed ionic/electronic conductivity and surface-controlled electrochemical reaction mechanism, which significantly enhances the performance of $LiNi_{0.8}Co_{0.15}Al_{0.05}O_2$ (NCA) electrode and improves the NCA-Nb_2O_5 battery. However, the effectiveness of P(NDI2OD-T2) is limited by its poor stability at low voltage.

The thesis of Kuan Zhai is approved.

Laurent Pilon

Aaswath Raman

Bruce Dunn, Committee Chair

University of California, Los Angeles

2022

Table of Contents

List of Figures

List of Tables

1. Background and Objectives

1.1 Introduction to Lithium Ion Batteries

Energy storage devices are key components for many modern electronic components, and the lithium ion batteries (LIBs) are considered an outstanding power source for these components due to their high energy and power density, stable working voltage and long cycle life. Therefore, LIBs have been widely used in electric vehicles, commercial electronic devices and grid storage systems, and the market for these items are expected to keep growing rapidly. The need for LIBs is projected to grow from approximately 300 GWh in 2020 to 2000 GWh by 2030 [1]. Obviously, the research interest for developing LIBs with better performance is strongly fueled by this demand.

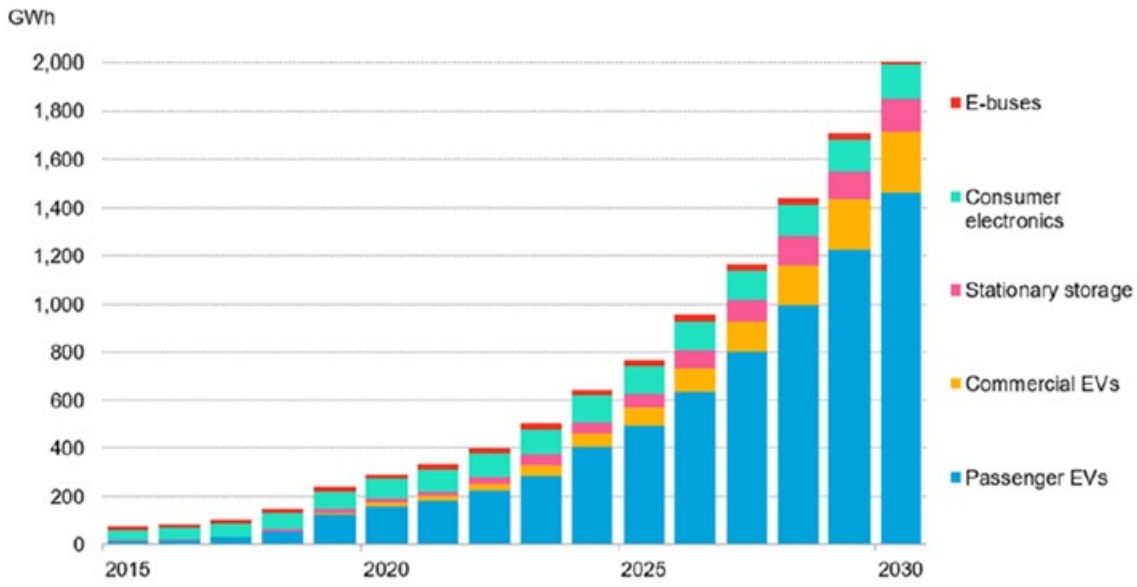

Figure 1.1 Worldwide anticipated use applications of LIBs [1].

In order to achieve the ideal battery performance, Lithium (Li) is investigated as one electrode due to its overwhelming advantages in Li-electrochemistry. The light molecular weight and small ionic radius contribute to the fast ionic diffusion, while the low redox potential [E°(Li+/Li) =−3.04 V vs standard hydrogen electrode (SHE)] offers high output voltage and energy density [2]. The demonstration of Li metal batteries by Whittingham in the 1970s was succeeded by Li-intercalation compound electrodes using $LiCoO_2$ (LCO) developed by Goodenough's group in 1980s. This electrode material increased the battery working voltage to 4.0 V from the previous Li metal result of 2.5 V [3][4]. Over the subsequent decades, various Li-intercalation compounds have been discovered as the active materials and used as either the cathode or anode.

The structure for a typical LIB is shown in the Figure 1.2, which consists of three main components: cathode, anode and electrolyte [5]. The Li ions migrate through the electrolyte between cathode and anode, which are working as the ion-host structures. During the charging process of the battery, lithium ions are extracted from the cathode, travel through the electrolyte, and finally are inserted into the anode. At the same time, electron flow follows the same direction, but travels through the external circuits. The discharging process reverses the directions of both the ion extraction/diffusion/insertion and the electron flow. Under this condition, the ion extraction/diffusion/insertion mechanisms are the dominant factors which determine the battery performance. Moreover, the electrode materials, where the extraction and insertion occur, become a critical challenge for the current research.

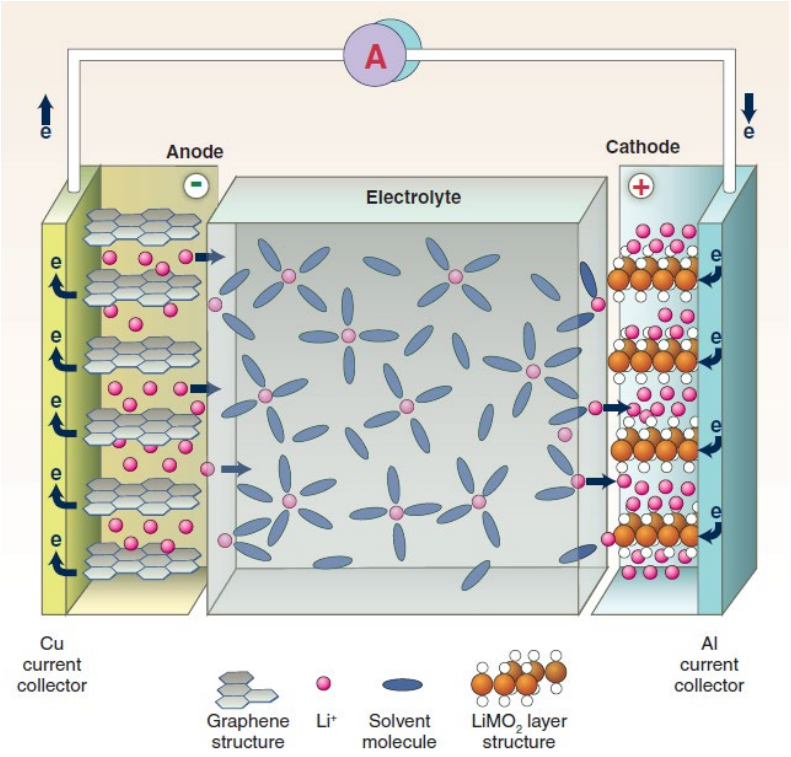

Figure 1.2 Schematic of a LIB [5].

1.2 Electrode Materials

The electrode is generally composed of three kinds of materials: active materials, conductive agents and binders. The active material is the main component involved in electrochemical reactions, and contributes to the battery capacity. The conductive agent, such as carbon black or carbon nanotubes, improves the electronic conductivity. It is especially essential if the electronic conductivity of the active material itself is low. Traditionally, a polymer binder is used in the electrode to hold the active material and conductive agent together, and bind all the components onto the metallic current collector.

The commonly used active materials in current research are listed in the Table 1.1, which are divided into two categories according to cathode and anode materials.

Electrode	Active Material	Specific Capacity (mAh/g)	Working Voltage (V vs Li/Li+)
Cathode	$LiCoO_2$ (LCO)	274	1.9
	$LiNi_{0.8}Co_{0.15}Al_{0.05}O_2$ (NCA)	279	3.7
	$LiFePO_4$ (LFP)	179	3.4
Anode	$Li_4Ti_5O_{12}$ (LTO)	175	1.55
	Nb_2O_5	180	1.6
	Graphite	372	0.07
	Si	4012	0.05

Table 1.1 Commonly used active materials on electrodes.

LCO has been used in commercialized products since 1991, and continues to dominate the LIB market for portable electronic devices because of its high specific capacity (274 mAh/g) and excellent stability during cycling [6]. However, its chemical stability at high voltage is a potential risk, which limits the output voltage of LCO batteries. LFP shows relatively lower capacity when compared to LCO, but the negligible volume variation during Li ion insertion/extraction process makes it much safer than the LCO [7]. NCA is considered an attractive cathode material for its high energy density and improved structural stability, however, its surface degradation and thermal stability are unsolved issues for practical applications [8][9].

As for the active materials for anodes. LTO is an attractive choice for both research and practical application for the LIB anode due to its 175 mAh/g specific capacity and extremely

long cycle life over several thousand cycles [10]. However, the 1.55 V working voltage makes it difficult to achieve a high output voltage battery since it requires much higher working voltage for the cathode. Nb_2O_5 shows similar performance to the LTO in terms of specific capacity and working voltage. However, it is considered as a potential option for fast charging/discharging batteries. Nb_2O_5 exhibits rapid and massive Li ion insertion/extraction without phase change due to preferred ion transport along specific crystallographic pathways, which leads to the high ionic conductivity [11][12]. Graphite has also been used as an anode material for decades because of its high reversible capacity of 372 mAh/g. But the relatively lower rate capability of graphite limits its use in fast charging/discharging LIBs [13]. Silicon is widely investigated as the replacement for graphite, because it is much cheaper than the graphite but achieves much higher capacity (4012 mAh/g) [14][15]. However, its poor conductivity and severe volume change in the lithiation/de-lithiation process remains a significant challenge [16].

1.3 Binder Materials

In order for batteries to store more energy, higher electrode mass loading is required, especially if the development of the active material specific capacity remains limited. However, thicker electrodes from high mass loading leads to challenges with other electrode components, specifically conductive agents and binders. The higher electrode thickness leads to longer distances for ion diffusion and electron transport, and higher ionic/electronic conductivity is required for the electrode in order to maintain the power density, cycle life and rate

performance. Additionally, thick electrodes tend to be more sensitive to the mechanical stress and broke easily from electrode volume changes associated with ion extraction/insertion during cycling. The polyvinylidene fluoride (PVDF) binder is commonly used in lithium-ion battery electrodes because of its electrochemical stability. However, PVDF has relatively poor ionic/electronic conductivity and limited mechanical integrity [17]. In contrast, conjugated polymers provide mixed ionic/electronic conductivity and promise mechanical strength at the same time, and are considered to be outstanding candidates as multifunctional binders [18][19][20].

The polymer binder is used to mix and hold all the electrode components together, including active materials and conductive agents. Thus, it is recognized as one of the critical parts for the electrode, even though it is used in a small mass ratio (usually 10% or less). The binder candidates for the LIBs require not only electrochemical stability and mechanical strength, but additional properties such as electronic/ionic conductivity and solubility in different solvents. The electrochemical stability and mechanical strength provide the basic adhesion function during the cycling process, which is widely required for traditional binders. The new multi-functional binders with better conductivity and solubility widen the choice of electrode active materials for improving the rate capability and cycling stability for LIBs. The choice of binder depends on the active materials used on the electrode because the electrochemical reaction of the active materials determines the working environment for the

binders. The different properties of the active materials raise questions about binder compatibility and lead to binder-based studies.

Among the various cathode materials, LCO has been widely commercialized and the resulting batteries are mostly fabricated with the PVDF binder due to its electrochemical stability in the battery and industrial-scale production. The current research for PVDF in LCO electrodes is mainly focus on PVDF crystallinity in order to reach a balance between the rate capability, cycling stability and the adhesion strength [21]. Other than PVDF, some binders, such as carboxyl methylcellulose/styrene-butadiene rubber (CMC/SBR), are also under investigation. The research direction with this system is to solve the stability problem of LCO at high voltage conditions [22]. LFP is another commonly used cathode material. It exhibits a negligible volume change during the charging/discharging process, and an extremely stable solid-electrolyte-interphase (SEI) layer can be formed in the voltage window for LFP battery product. Therefore, the candidate binders for LFP electrode a high electrical conductivity, water-solubility and lower cost. Researchers have already indicated that polytetrafluoroethylene (PTFE), CMC, polyacrylic acid (PAA) exhibit better performance than PVDF [23][24][25]. Some research indicates that functionalized sodium alginate (SA) with 3,4-propylenedioxythiophene-2,5-dicarboxylic acid (ProDOT) provides better conductivity and adhesion strength [26]. The high working voltage of high-nickel cathode materials such as $LiNi_{1-x}M_xO_2$, including $LiN_{0.8}Mn_{0.1}Co_{0.1}O_2$ (NMC811) or $LiNi_{0.8}Co_{0.15}Al_{0.05}O_2$ (NCA), challenges the stability of traditional PVDF binder when they are charged to 4.3 V or higher,

while moisture-sensitive high-nickel containing cathode materials limit the use of aqueous polymer binders. Research has shown that replacing the PVDF binder with polyimide (PI) binder significantly improves the NMC811 battery performance and the high conductivity of polyaniline (PANI) is able to enhance the rate capability and cycling stability for $LiNi_{0.94}Co_{0.06}O_2$ batteries [27][28].

In studies involving the LTO anode, binder design concentrates more on structural stability and rate capability at high mass loading, which requires higher adhesion strength and conductivity. The influence of the binder on interfacial properties, such as SEI formation, is also being investigated in order to determine the electrochemical stability of the LTO working voltage window. Research has shown that water-soluble binders, such as CMC and PAA, exhibit enhanced electrochemical performance in LTO cells [28][29]. In addition, graphite has been widely used as the LIB anode in commercialized products for decades in conjunction with PVDF or CMC/SBR binders. In this case, research has confirmed that CMC/SBR binder is involved in slowing down the graphite SEI layer formation, so that CMC/SBR binder shows better cycling stability than the PVDF binder [30]. Moreover, PVDF might react with Li metal or lithiated graphite at high temperature (above 45 °C), which leads to severe safety issues [31]. Some research has emphasized the modification of PVDF and a ternary binder, PVDF-polymethylmethacrylate (PMMA)-poly (lithium methacrylate (PMALi), has been developed which shows significant improvement at an extremely high 50 C rate. The ternary binder maintains 96.2% of capacity while pure PVDF maintains 16.2%) [32]. Another direction has

been to develop bio-derived polymers such as alginate, chitosan, guar, xanthan, and polysaccharides. These binders have shown enhancement on battery performance compared to PVDF, [33].

Table 1.2 Active materials and binders.

Electrode	Active Material	Properties/Demands	Binder
Cathode	LCO	Excellent cyclic stability Poor electrochemical stability at high voltage	PVDF, modified crystallinity for ionic conductivity CMC/SBR, improve the stability at high voltage
	LFP	Negligible volume change Stable solid-electrolyte-interphase (SEI) layer	PTFE, CMC, PAA, water-solubility and lower cost ProDOT, better ionic/electronic conductivity
	NCA	High working voltage Moisture-sensitive	PI, PANI, ProDOT, conductivity
Anode	LTO	Long cycle life Harmful SEI layer Poor conductivity	CMC and PAA, improve interfacial properties
	Graphite	High capacity Safety issue at high temperature, 45℃	CMC/SBR, slow down SEI layer formation, improve cyclic stability PVDF-PMMA-PMALi, stability at high temperature, improve rate capability

1.4 Research Objectives

This work was supported by the Center for Synthetic Control Across Length-Scales for Advancing Rechargeables (SCALAR), an Energy Frontier Research Center Two series of conductive binders, the 3,4-propylenedioxythiophene-2,5-dicarboxylic acid family (ProDOT)

and poly{[N,N′-bis(2-octyldodecyl)-naphthalene-1,4,5,8-bis (dicarboximide)-2,6-diyl]-alt-5,5′-(2,2′-bithiophene)} family (P(NDI2OD-T2)), were synthesized in Professor Barry C. Thompson's group at the University of Southern California. Those polymers are considered to be the conductive binder candidates for the LIB cathodes and anodes, respectively, due to their conjugated structures. According to theoretical guidance and preliminary experiments, the ProDOT binder is paired to an NCA cathode and P(NDI2OD-T2) is paired to the LTO anode. In this thesis, each of the two polymers will be investigated for their own electrochemical properties, their influence on LIB electrodes, and the performance when being used as the binders for LIBs.

Chapter 2 will introduce the current research on the ProDOT and P(NDI2OD-T2) binders and the experimental setting for this thesis. The fabrication of sample electrodes of NCA-ProDOT cathodes and LTO- P(NDI2OD-T2) anodes is demonstrated in this chapter along with polymer thin film electrodes. The details for the electrochemical experiments for the thin film electrodes and coin cells are also included in this chapter.

Chapter 3 will show the experimental results on ProDOT binders. The polymer thin film electrodes are tested in three electrode experiments in order to investigate the electrochemical properties and mechanisms of the pure polymer itself. Coin cell experiments on NCA-Li metal half-cells and NCA-Nb_2O_5 full cells are presented. The ProDOT binder used in the NCA cathodes is compared to the PVDF binder. The evaluation of the ProDOT is based on both the pure polymer performance s and how the polymer functions as the cathode binder.

Chapter 4 will present the experimental results for P(NDI2OD-T2). Similar experimental procedures were used as those in Chapter 3. The polymer properties are investigated in thin film three electrode cells while coin cell experiments carried out for P(NDI2OD-T2) in LTO anode are compared to PVDF binders in the LTO half-cells. Due to poor performance in the half-cell experiments, full-cell experiments with the P(NDI2OD-T2) binder were not investigated. The performance of the P(NDI2OD-T2) polymer on its own and how it influences the LTO anode in half-cells is discussed.

Finally, the chapter 5 summarizes the research of this thesis and identifies future research directions.

2. Introduction to the experiment

2.1 Polymer binder

The ProDOT family of materials is considered to be an alternative polymer to the poly(3-alkylthiophenes) (P3AT) and poly(3,4-ethylenedioxythiophene) (PEDOT) families as the latter two conjugated polymer binders have exposed their shortcomings, which reported on the previous studies in our program for the LIB cathode binders [20]. The P3AT family shows outstanding electronic conductivity because of the relatively narrow band gap and high hole mobility. In addition, the fabrication of electrodes when using this polymer also benefited from its good processability and solubility. However, the dense chain packing structure limits the Li+ ion diffusion and eventually leads to low ionic conductivity. The electrochemical stability

is also challenged by the demand for cathode active materials with high working voltage. As for the PEDOT family, it has shown excellent stability when coated on LIB cathodes and led to improved cycling behavior. However, the intrinsically insoluble PEDOT systems result in poor uniform thin film coating, which hinders electrode fabrication. As a result, the ProDOT family becomes attractive due to its beneficial properties. The propylenedioxythiophene backbone contributes to the ProDOT electrochemical stability and allows repeated cycling over a wide voltage window from 3.0 V to 4.5 V. The hexyl side chains lead to improved solubility in nonpolar solvents and result in the better processability for the electrodes. The alkylenedioxy bridge structure on the side chains not only enhanced the solubility in organic solvent, but also reduced the onset voltage for oxidation and increased the electronic conductivity due to the electron donating oxygen atoms. In addition, the partly disordered morphology in the less crystalline ProDOTs is helpful for the Li+ ion insertion/extraction, facilitating ionic conductivity. Combining all the above features, the ProDOT family shows favorable mixed ionic and electronic conductivity with very good stability over a wide voltage window. These properties are beneficial for electrode rate capability and cycling performance [20]. Additionally, the solubility in nonpolar organic solvent provides good processability, and is compatible with electrode fabrication.

The ProDOT family of polymers used in this dissertation were provided by Professor Barry C. Thompson's group in University of Southern California. The direct arylation polymerization (DArP) method (shown in Figure 2.1) is used for the polymer synthesis in order to prevent the toxic, unstable, and hard to purify metalated monomers typically used in

traditional cross-coupling reactions. The DArP method activates the C-H bond and allows it to reacts with aryl halide C−X bond to form the C−C bond, and no extra synthetic step is required for the ProDOT synthesis. The ProDOT product is synthesized with a number-average molecular weight (M_n) of 19.1 kDa and a dispersity of 1.6. According to previous research on the same ProDOT, the polymer shows excellent mixed ionic and electronic conductivity as expected. The ionic conductivity achieves 10^{-7} S/cm and the electronic conductivity achieves 0.1 S/cm over the 3.0~4.2 V voltage window.

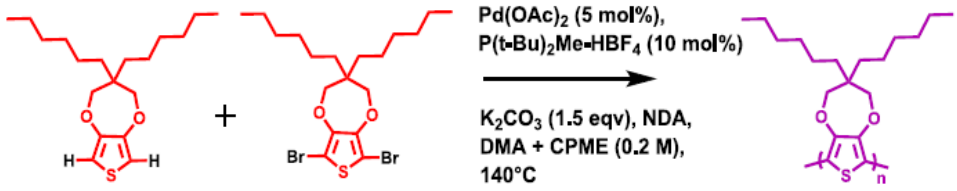

Figure 2.1 Synthesis of ProDOT using DArP method [20].

Different from the p-dopable polymers for cathode binders described above, the anode binders require n-dopable polymers. In general, n-dopable polymers and their electron-transport have received relatively less interest compared to the p-type. poly{[N,N′-bis(2-octyldodecyl)-naphthalene-1,4,5,8-bis(dicarboximide)-2,6-diyl]-alt-5,5′-(2,2′-bithiophene)} (P(NDI2OD-T2)) was introduced by Facchetti's group in 2009 [34]. The P(NDI2OD-T2) consists of naphthalene dicarboximide (NDI) acceptor and bithiophene (T2) donor subunits, and shows very good performance when used as a n-type semiconducting polymer. The electron mobility achieves 0.85 cm^2/Vs along the chain direction, and maintains high performance stability under ambient conditions. The solution processability and high crystalline nature are also advantageous for electrode fabrication. However, the P(NDI2OD-

T2) polymer tends to form aggregates in several specific solvents, which results in the harmful phase separation [35].

The P(NDI2OD-T2) family of polymers used in this dissertation were also provided by Professor Thompson's group. The synthesis process is shown in Figure 2.2, and the product P(NDI2OD-T2) has a quantitative yield with M_n = 37.4 kg/mol and PDI = 3.5. In the previous research on the polymer synthesized in the same group, the undoped P(NDI2OD-T2) polymer shows ionic conductivity of 3×10^{-10} S/cm and electronic conductivity of 5×10^{-7} S/cm. Both the ionic and electronic conductivities improve with the increased doping level during cycling, and eventually reach 6×10^{-9} S/cm and 5×10^{-4} S/cm respectively [36]. Thus, the P(NDI2OD-T2) polymer is considered as a possible candidate for anode binders in LIBs due to the excellent mixed ionic/electronic conductivity when used with an appropriate electrolyte solvent.

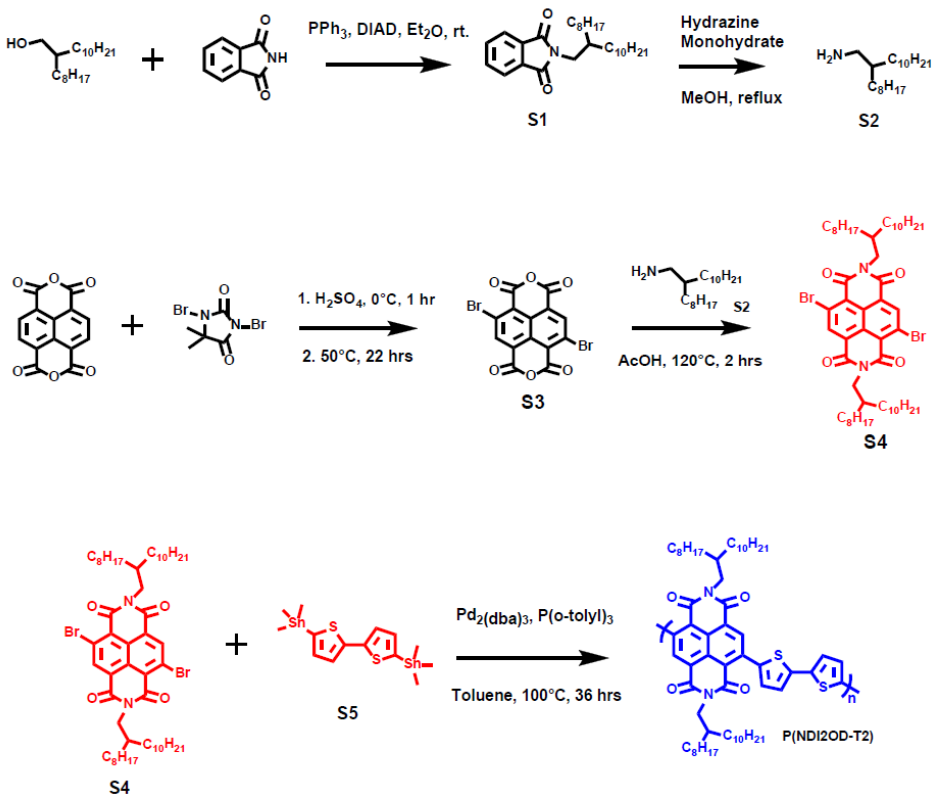

Figure 2.2 Synthesis of monomer and polymer P(NDI2OD-T2) [36].

2.2 Thin film three-electrode experiments

Fabrication of polymer thin film. All the polymer binders are dissolved in 1,2-dichlorobenzene (ODCB) at concentrations of 20 mg/mL. For each thin film electrode, 80 μL polymer solution is spin-coated on a 1cm × 2cm fluorine doped tin oxide (FTO) coated glass substrate, and the spin coating is set at 3000 rpm for 60 s. Then prepared samples are dried in the fume hood at room temperature for 2 h before transferred into the vacuum oven, in order to prevent the unevenness or cracks which result from the rapid drying. The remaining drying process is done in a 110℃-vacuum oven for 12 h, and the final products are the 100 nm polymer thin films which are coated on the FTO glass substrate. Figure 2.3 shows the polymer binder coated FTO conductive glasses.

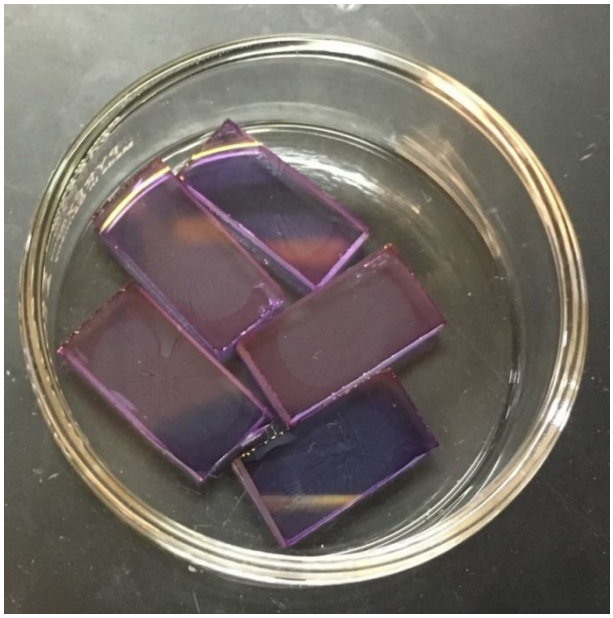

Figure 2.3 Polymer binder coated FTO conductive glasses.

The three-electrode cell arrangement. The dried thin film samples are moved into a glovebox for the three-electrode experiments where they serve as the working electrodes (shown as Figure 2.4). The polished Li metal foil is used as both counter electrode and reference electrode, while the electrolyte is chosen to be the 1 M LiTFSI in EC: DMC at 1:1 ratio solution. The electrochemical reaction will occur between the working electrode and the counter electrode, while the reference electrode provides a stable reference for the parameter measurement.

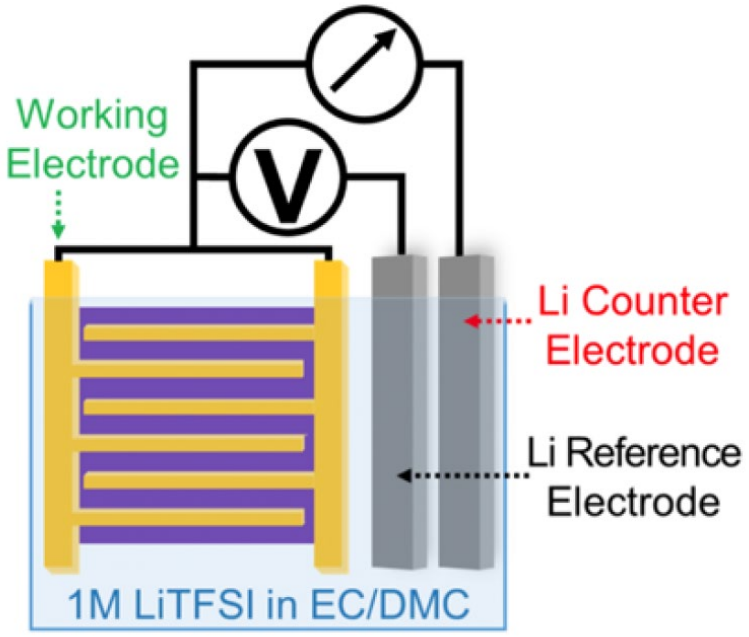

Figure 2.4 Schematic of the three-electrode experiment.

2.3 Coin cell experiments

Fabrication of coin cell electrodes. The NCA electrodes for cathodes are prepared with a slurry mixture which contains NCA particles, Super P, carbon nanotube (CNT) and binder in a weight ratio of 90:3:3:4. The 20 mg/mL ProDOT-ODCB solution is used for the experimental results and the 20 mg/mL PVDF-NMP solution is used as the control group. The powder mixture of NCA, Super P and CNT was finely ground by mortar and pestle before adding the binder solution. NMP was then added to adjust the slurry viscosity before the NCA slurry was cast on Al foil with a 1 mg/cm^2 mass loading. Finally, the cast sample is dried in the fume hood at room temperature for 4 h and then in a 110℃-vacuum oven for 12 h.

The LTO electrodes for anode are prepared with a slurry mixture which contains LTO particles, Super P, carbon nanotube (CNT) and binder, using the same 90:3:3:4 mass ratio as that used in cathode slurry. The P(NDI2OD-T2)-ODCB solution was used for the experimental results with the same PVDF-NMP solution used for control group. The slurry mixture was cast on Cu foil instead of Al foil because the Al substrate cannot be used on anode side at the low voltage in this experiment. All the other procedures are the same as those for the NCA electrode fabrication.

The Nb_2O_5 electrodes consist of Nb_2O_5 which have been coated with reduced graphene oxide (Nb_2O_5-rGO) and PVDF at a 9:1 mass ratio. There are no other conductive carbon additives used in the mixture because the rGO which coated the Nb_2O_5 particles contribute to

the conductivity. This anode material is cast on Cu foil with the 2 mg/cm^2 mass loading in order to balance the theoretical capacity between the cathode and anode.

Packaging of the coin cells. The prepared electrodes were placed into the coin cell along with stainless spacers (current collectors) and glass fiber (separator). The same 80 μL 1 M LiTFSI in EC: DMC at 1:1 ratio electrolyte is dropped onto the separators in each coin cells.

The coin cells were divided into two different groups, half-cells and full-cells, depending on the counter electrodes used. The half-cells for both NCA-ProDOT and LTO- P(NDI2OD-T2) coin cell use Li metal foil as the counter electrode because the excess Li will not limit the behavior of the testing materials. The NCA-ProDOT full-cell experiments use the Nb_2O_5 electrode.

2.4 Experiment design

The thin film samples were tested in a glovebox and the coin cells were tested in the air. All the experiments were done using a VMP potentiostat/galvanostat (Bio-Logic).

Cyclic Voltammetry (CV) experiment. CV experiments consist of scanning linearly the potential of the stationary working electrode. As the potential sweeps, the potentiostat measures the current resulting from electrochemical reactions. TCV experiments at different voltage ranges are done first on each material in order to confirm the material stability and available voltage ranges.

In order to analyze the kinetics of polymer doping/dedoping, CV results with different sweep rates are required. The measured currents (i) and scan rates (v) follow the equation:

$$i = av^b$$

where the b value analysis at those redox peaks represents the kinetics of the reactions. A b value close to 0.5 results from a process controlled by diffusion, while a b value equal to 1.0 indicates a non-diffusion controlled or a surface-controlled charge-storage process.

The CV experiments for thin film samples use 10~100 mV/s scan rate while the coin cells use 0.1~1.0 mV/s rate, because lower sweep rates minimize the shifts of redox peaks associated with polarization. At sweep rates higher than 100 mV/s, redox peak shifts from polarization lead to inaccuracy of the b value analysis.

The voltage ranges for CV experiments are determined by the properties and uses of the materials. The binders need to be stable at the voltage where the active materials, NCA on cathodes and LTO on anodes, are redox active during cycling. The CV experiments on cathode binder ProDOT starts from 3.0 V and ends at 4.2 V or higher, while the anode binder P(NDI2OD) is scanned from 3.0 V to 1.5 V or lower (all voltages are with respect to Li/Li+)

Galvanostatic Voltammetry (GV) experiment and C rate experiment. In GV and C rate experiments, the sample cells are charged and discharged at constant current within certain potential ranges. For the thin film samples, the GV experiments are analyzed based on a series

of currents from 1 to 100 μA. The coin cells, including both half-cells and full-cells, are tested at C rates from C/2 to 5C, which covers both low-rate and high-rate charging. The 1C rate for both NCA and LTO coin cells are chosen to be 160 mA/g, which was determined by the control experiments at low-rates of cycling.

3. Performance of conductive polymer ProDOT as cathode binder

3.1 Results and discussion of thin film three electrode experiment

Both Hexyl-ProDOT and (75:25) (Hex:OE)-CoProDOT thin film samples are tested in three-electrode cells, in order to analyze the performance in CV and GV experiments. The properties of the pure polymer are shown in these thin film sample experiments without any other additive agent but only the polymer itself.

Figure 3.1 (a) shows the electrochemical doping and dedoping for Hexyl-ProDOT thin film samples. This CV experiment is done between 3.0 and 4.2 V with sweep rates varying from 40 to 100 mV/s. The CV curves show two pairs of charging and discharging peaks, which are located at 3.23 V and 3.80 V when charging, 3.16 V and 3.62 V when discharging. These charging and discharging peaks represent the voltages where the electrochemical reactions occur while the two separate pairs of peaks indicate two different doping/dedoping processes polaron and bipolaron. With increasing scan rate, each redox peak shifts slightly to high potential region when charging and to low potential region when discharging. The differences

are all smaller than 0.005 V, and the minimal amount of peak shifting indicates that these are high-rate processes.

The peak currents used for b value calculation are shown in the Figure 3.1 (b). According to the results, during the charging reactions, the first peaks at 3.23 V for the polaron reaction has the b value of 0.96, and the second peak at 3.80 V for the bipolaron reaction has a smaller b value of 0.86. Similarly, b=0.92 at the first reaction peak when discharging to 3.62 V, and b=0.86 at the second reaction peak when discharging to 3.16 V. These four b values are close to 1.0 indicating that the doping and dedoping reactions are mostly under surface control, which results from both the material properties and the thin-film structure. In addition, the small reduction in the b values between the first reaction and second reaction for both charging and discharging process respectively, may occur from the depletion of ions within the surface layer. In summary, the b value analysis shows that a rapid redox process occurs in the polymer thin films, and the fast kinetics for the electrochemical doping/dedoping of Hexyl-ProDOT are expected to facilitate rapid charge transfer when used as the conductive binders in cathodes. The fast doping/dedoping process in Hexyl-ProDOT makes it a good candidate choice for the conductive binder.

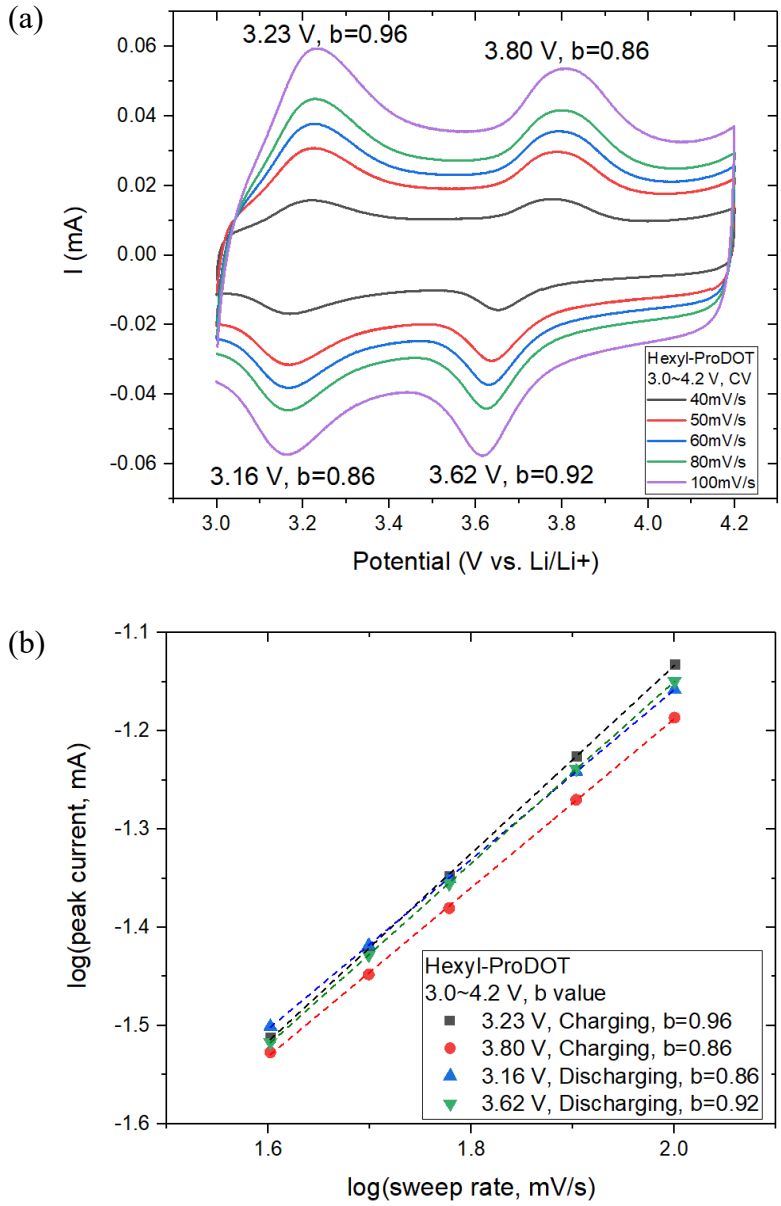

Figure 3.1 CV experiment data for Hexyl-ProDOT thin film. (a) CV curves for Hexyl-ProDOT thin film cycled with a potential window ranging from 3.0 to 4.2 V vs. Li/Li+ as a function of various sweep rates from 40 to 100 mV/s. (b) The b value analysis at the current peaks basing on the log of the peak current (i) versus log of the sweep rate (v) for the data shown in (a).

Figure 3.2 (a) shows the CV cycling in the 3.4~4.2 V voltage range, which includes only the bipolaron process. The CV curves within this smaller range show that the bipolaron reactions occur without have the polaron reaction precede it. The bipolaron charging and discharging peaks occur at higher voltage, 3.85 V and 3.58 V respectively. Since the measurements were carried out on the same sample as that in Figure 3.1-1 (a), the slight peak shifts (50 mV or so) may result from material degradation from the extended cycling. It can also be confirmed that those two peaks located at lower voltages represent the doping/dedoping in polaron procedures.

Figure 3.2 (b) shows the b value analysis for the CV curves in the 3.4~4.2 V range. The values of b=0.85 at 3.85 V and b=0.91 at 3.58 V match with b value analysis results for the 3.0~4.2 V range, which are 0.86 and 0.92 respectively. This similarity indicates that the surface control mechanism for the bipolaron reactions is not influenced by whether there are polaron dopants. Thus, there will not be too much difference in redox properties between full-charge/discharge and partial-charge/discharge for this polymer binder.

(a)

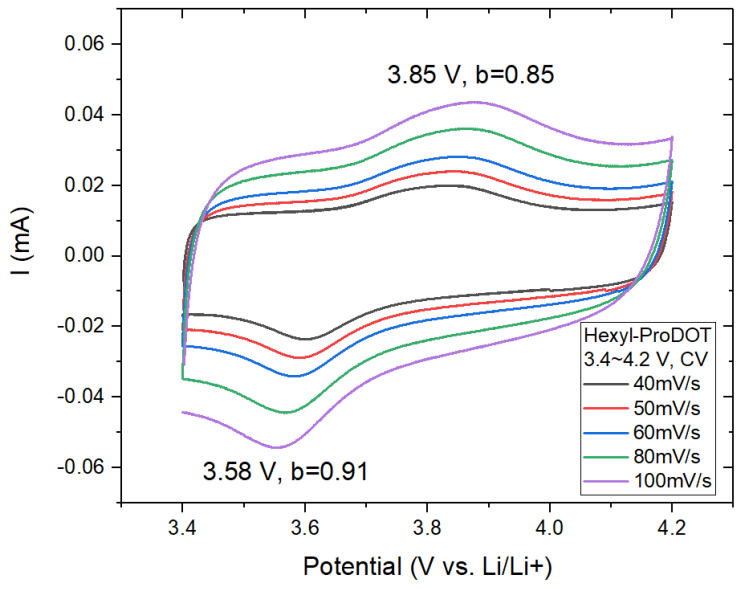

(b)

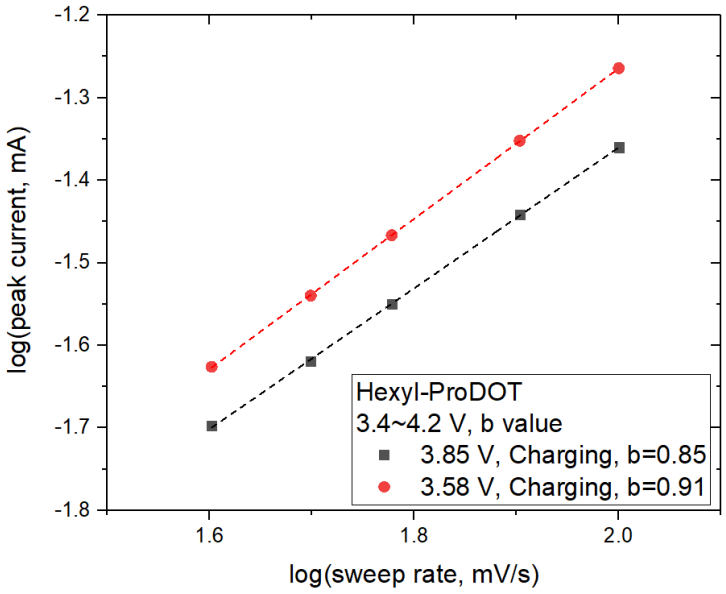

Figure 3.2 CV experiment data for Hexyl-ProDOT thin film. (a) CV curves for Hexyl-ProDOT thin film cycled with a potential window ranging from 3.4 to 4.2 V vs. Li/Li+ as a function of various sweep rates from 40 to 100 mV/s. (b) The b value analysis at the current peaks basing on the log of the peak current (i) versus log of the sweep rate (v) for the data shown in (a).

The GV experiments for the Hexyl-ProDOT thin film samples are shown in the Figure 3.3. Figure 3.3 (a) represents scanning in the 3.0~4.2 V range, while Figure 3.3 (b) represents the 3.4~4.2 V bipolaron range. Because the thin film mass loading cannot be measured accurately, the 2μA current was estimated to correspond to 1C condition based on capacity calculation in in previous CV experiments.

According to the Figure 3.3 (a), the hexyl-ProDOT thin film sample shows a capacity of 0.112 μAh and 0.088 μAh when charging and discharging at the 2 μA rate respectively. The

capacity decreases with increasing rate; the capacity drops to 0.014 μAh at 100 μA (approximately 50C rate). Although the degradation of capacity occurs, the hexyl-ProDOT still retains nearly 50% capacity (0.045 μAh) at 20 μA (approximately 10C rate). This is an extremely high value for a conductive binder material. There are, however, capacity gaps between charging and discharging in each cycle. These capacity differences may be the result of irreversible reactions at high voltage, which might suggest limitations in the polymer stability at high voltage. In addition, the capacity gaps tend to be smaller at higher current rates, and the capacity gap becomes less than 0.005 μAh when it comes to 20 μA rate. The irreversible reactions seem to be saturated after several cycles, and the limited reaction time may also contribute to reducing the irreversible reactions.

The GV experiments carried out in the bipolaron range at 3.4~4.2 V (Figure 3.3.b) are similar to the CV experiments shown in Figure 3.1-2. The 2 μA rate cycling experiments show 0.051 μAh capacity when charging and 0.040 μAh when discharging, which are nearly half the capacity shown in the 3.0~4.2 V range. This capacity ratio is roughly consistent with the CV curves shown previously in Figure 3.2 and 3.1. Additionally, the capacity degradation is much more severe in the 3.4~4.2 V range compared to that in the 3.0~4.2 V range. In the bipolaron range, there is only 25% capacity remaining at 20 μA, and the capacity decreases to almost zero at a current of 40 μA. However, between 50% and 30% capacity remains at the same rates in the 3.0~4.2 V range. The significant difference indicates that the bipolaron process is highly

limited at higher charging and discharging rates. The GV results support that the hexyl-ProDOT is able to contribute to the cathode capacity although it is a very small amount.

(a)

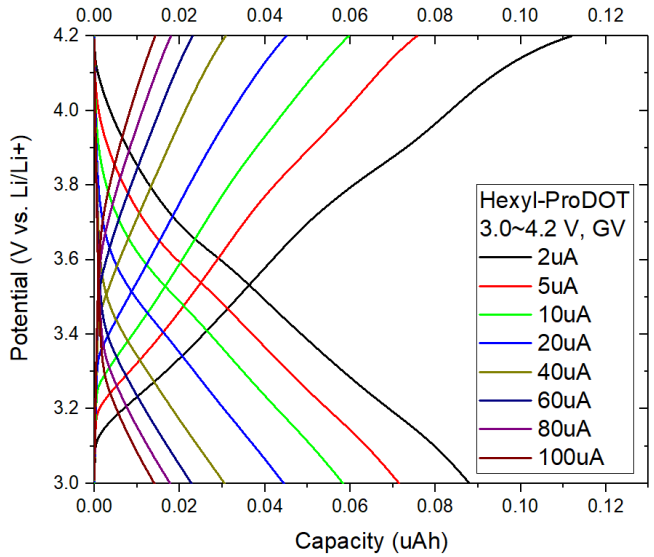

(b)

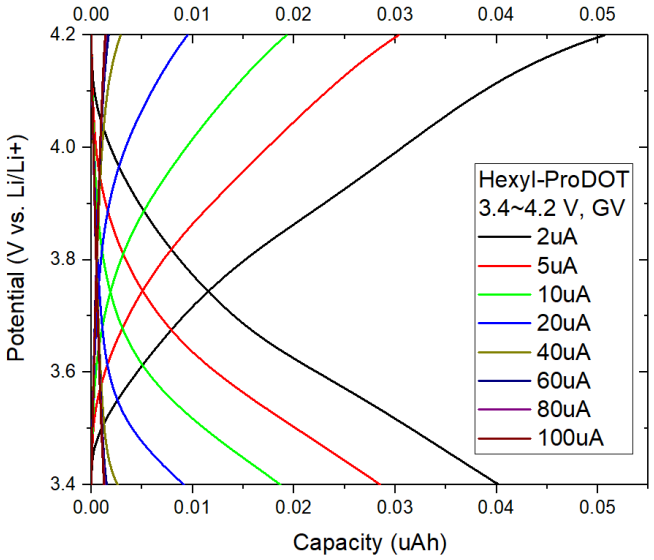

Figure 3.3 GV experiment data for Hexyl-ProDOT thin film. (a) GV curves for Hexyl-ProDOT thin film cycled with a potential window ranging from 3.0 to 4.2 V vs. Li/Li+ as a function of various current from 2 to 100 μA. (b) GV curves for Hexyl-ProDOT thin film cycled with a potential window ranging from 3.4 to 4.2 V vs. Li/Li+ at the same current condition.

Figure 3.4 shows the CV experiments on (75:25) (Hex:OE)-CoProDOT thin film samples, with the same electrochemical doping/dedoping which was done with Hexyl-ProDOT. The experiment is carried out under the same 3.0~4.2 V potential range and 40~100 mV/s scan rate. The CoProDOT CV curves also show two pairs of charging/discharging peaks, which can be distinguished easily. The charging peaks are located at 3.25 V and 3.81 V, while the discharging peaks are located at 3.17 V and 3.62 V. The similar polaron/bipolaron peak pattern shown in both CoProDOT and Hexyl-ProDOT support that the ion insertion mechanisms remain the similar regardless of the oligoether (OE) side chain modification. The same low level of peak shifting, both less than 0.05 V from the lowest scan rate to highest scan rate, indicate that both polymers exhibit fast redox reactions. Although small voltage differences exist between the same peaks of CoProDOT and Hexyl-ProDOT, it is not that significant because all the potential gaps are less than 0.02 V.

The current values for the charging and discharging peaks are used for b value analysis and the results are shown in Figure 3.4 (b). From the calculation, b=0.91 at 3.25 V and b=0.82 at 3.81 V for the charging peaks, while b=0.90 at 3.62 V and b=0.83 at 3.17 V in the discharge peaks. The high b values represented in the CoProDOT 3.0~4.2 V CV cycling indicates that the polaron/bipolaron reactions are mostly surface controlled, which was the same result for the Hexyl-ProDOT. Additionally, the decrease in b value at the second peak when charging or discharging can also be detected in the CoProDOT experiments. The b value analysis indicates that the CoProDOT exhibits a similar doping/dedoping mechanism as that of Hexyl-ProDOT. However, the b values at each peak in CoProDOT CV experiments are somewhat lower than

the b value in Hexyl-ProDOT peaks at a similar position. The small b value differences (around 0.2~0.5) suggests that the oligoether (OE) side chain modification leads to more diffusion control reaction.

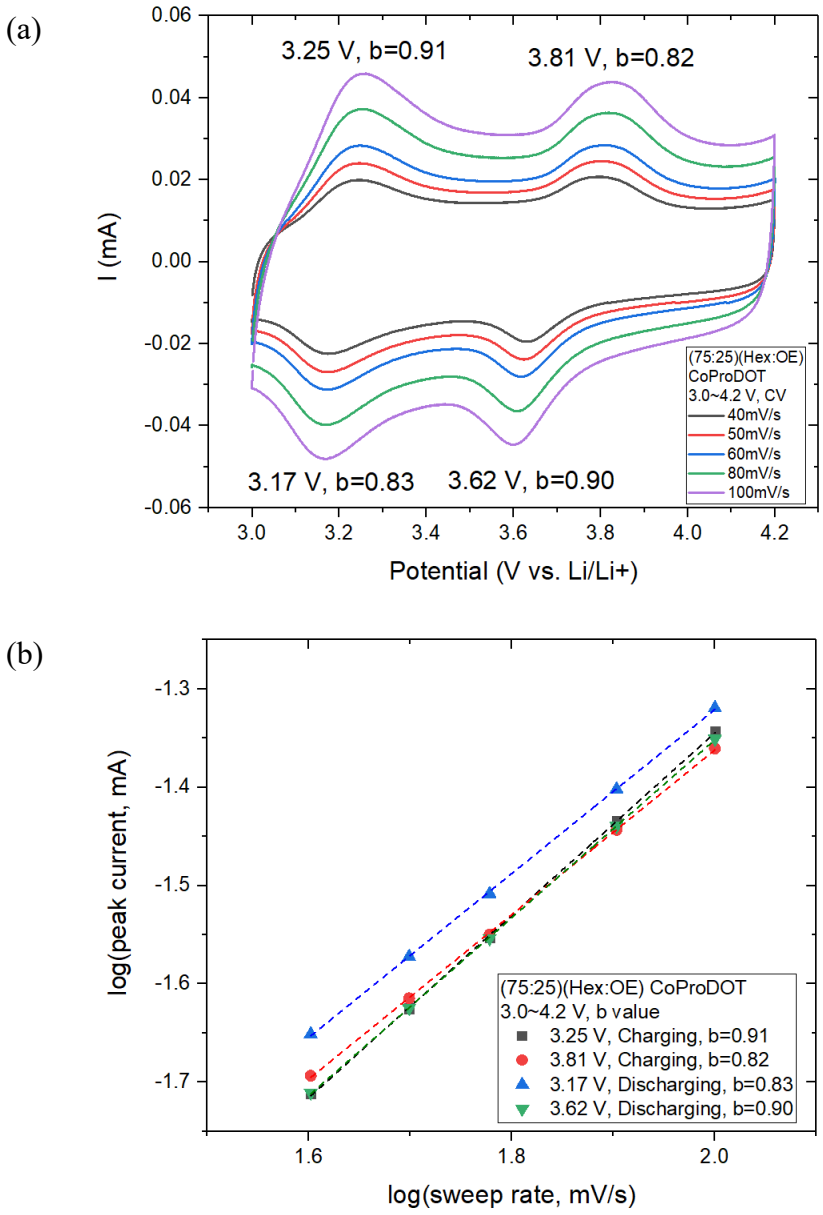

Figure 3.4 CV experiment data for (75:25) (Hex:OE)-CoProDOT thin film. (a) CV curves for Hexyl-ProDOT thin film cycled with a potential window ranging from 3.0 to 4.2 V vs. Li/Li+

as a function of various sweep rates from 40 to 100 mV/s. (b) The b value analysis at the current peaks basing on the log of the peak current (i) versus log of the sweep rate (v) for the data shown in (a).

Figure 3.5 (a) is the result of the CV cycling at 3.4~4.2 V voltage range, which was done in the bipolaron range without the polaron reaction. The existence of charging and discharging peaks indicate that the 3.87 V charging peak and 3.57 V discharging peak represent the bipolaron process, and the peak pair shown in 3.0~4.2 V at lower potential represents the polaron reaction. Compared to the bipolaron peaks shown in the Figure 3.1-4 (a), the charging peak slightly shifted to higher potential and the discharge peaks shifted to lower potential. This phenomenon remains the same as that in the Hexyl-ProDOT CV experiment, which may be the result of material degradation after extended cycling.

Figure 3.5 (b) gives the b value analysis for the current peaks in Figure (a). The b value is calculated to be 0.81 at 3.87 V for the charging peak and 0.88 at 3.57 V for the discharging peak. The surface-controlled nature of the redox process is not influenced by the changing of potential range. Moreover, the b value result for CoProDOT in the bipolaron range seems to be similar to the Hexyl-ProDOT for the same condition; 0.85 when charging and 0.91 when discharging. Thus, the oligoether (OE) side chain modification did not make significant difference in the CV experiments.

(a)

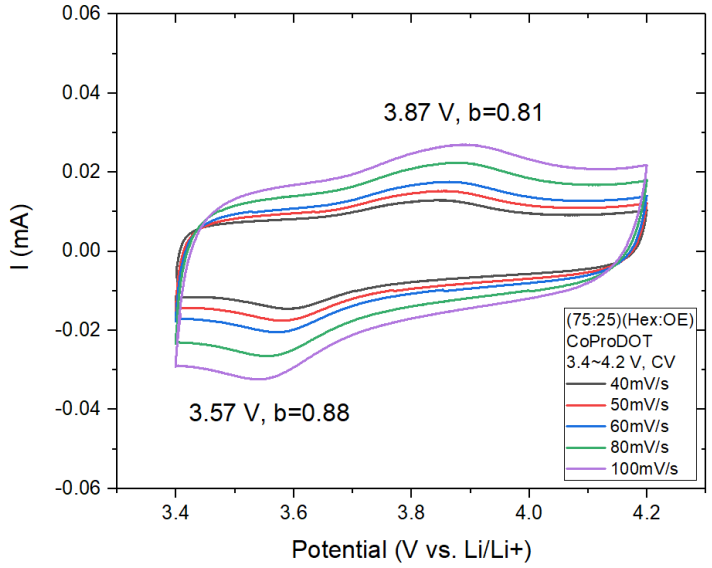

(b)

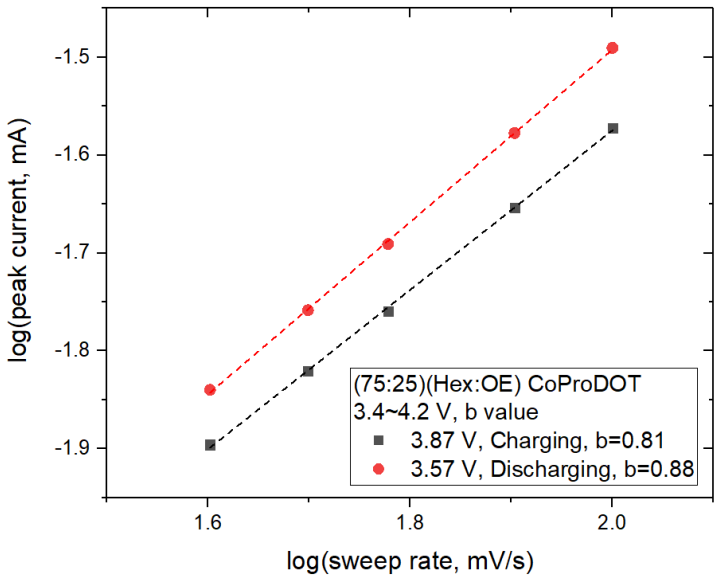

Figure 3.5 CV experiment data for (75:25) (Hex:OE)-CoProDOT thin film. (a) CV curves for Hexyl-ProDOT thin film cycled with a potential window ranging from 3.4 to 4.2 V vs. Li/Li+ as a function of various sweep rates from 40 to 100 mV/s. (b) The b value analysis at the current peaks basing on the log of the peak current (i) versus log of the sweep rate (v) for the data shown in (a).

The GV experiments for the (75:25) (Hex:OE)-CoProDOT thin film samples are shown in the Figure 3.6, Figure 3.6 (a) represents the GV scans in the 3.0~4.2 V range, and Figure 3.6 (b) shows the 3.4~4.2 V range for the bipolaron process. The 2μA current condition was estimated to correspond to the 1C rate based on former CV experiments.

In Figure 3.6 (a), the CoProDOT thin film sample shows a capacity of 0.109 μAh when charging and 0.086 μAh when discharging. The capacity tends to decrease at the higher current rate. Although the capacity drops to 0.03 μAh at 100 μA (approximately 50C rate), it remains 55% capacity (0.055 μAh) at the 20 μA condition (approximately 10C rate), which is slightly higher than the 50% retention in Hexyl-ProDOT GV experiments. However, the similar capacity gap between charging and discharging in each cycle can still be observed in CoProDOT GV curves. The CoProDOT might exhibit a similar irreversible reaction as that which occurs for Hexyl-ProDOT.

Figure 3.6 (b) shows the CoProDOT GV experiments in the bipolaron range, 3.4~4.2 V. The GV curves shows similar as that exhibited in the Hexyl-ProDOT GV experiments. The 2 μA cycles in the bipolaron range with nearly half of the capacity of the 3.0~4.2 V full-range (0.051μAh and 0.040μAh when charging and discharging respectively). The capacity degradation in the bipolaron range is much more significant than the 3.0~4.2 V range as the capacity drops to almost 0 at 60 μA in the bipolaron range while the 3.0~4.2 V full-range retains 0.023 μAh at the same current.

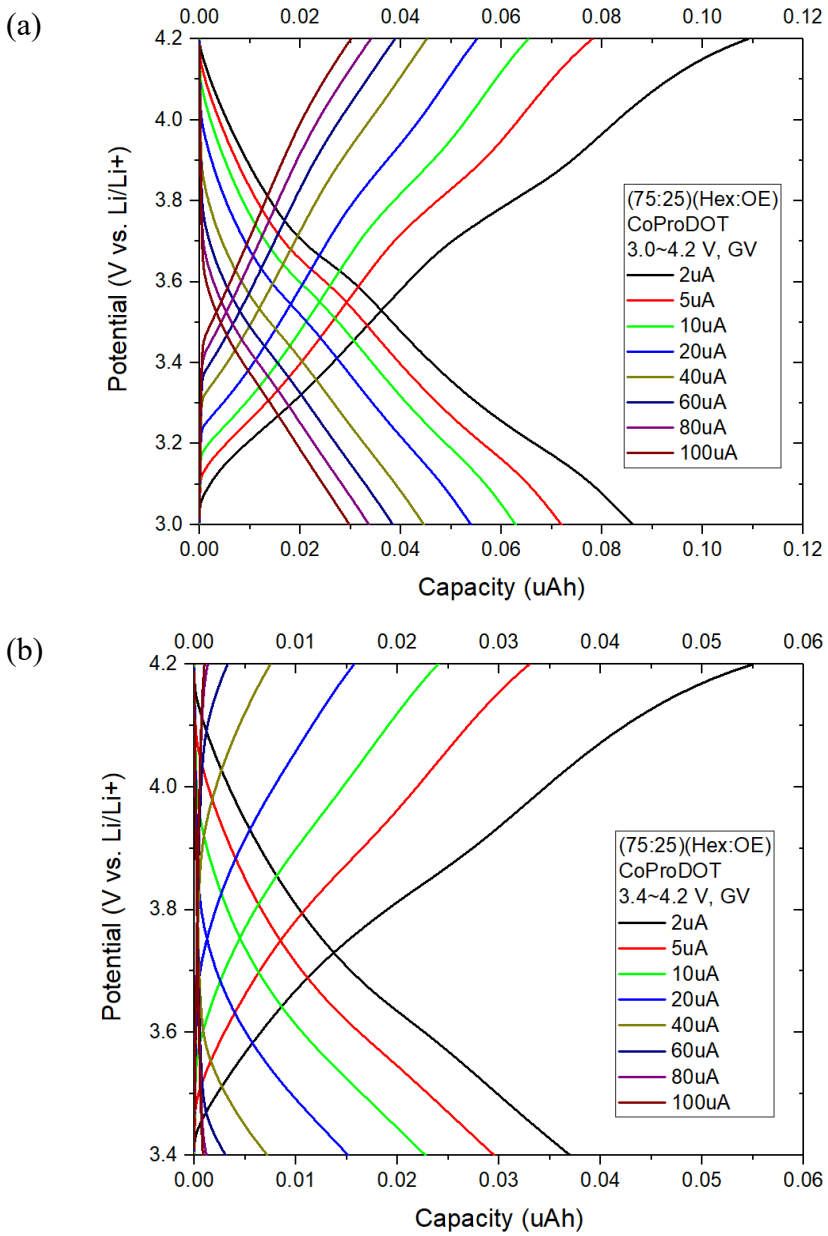

Figure 3.6 GV experiment data for (75:25) (Hex:OE)-CoProDOT thin film. (a) GV curves for (75:25) (Hex:OE)-CoProDOT thin film cycled with a potential window ranging from 3.0 to 4.2 V vs. Li/Li+ as a function of various current from 2 to 100 μA. (b) GV curves for (75:25) (Hex:OE)-CoProDOT thin film cycled with a potential window ranging from 3.4 to 4.2 V vs. Li/Li+ at the same current condition.

3.2 Results and discussion of half-cell experiment

Figure 3.7 shows the NCA half-cell experiments with different binders (Hexyl-ProDOT and PVDF) along with data from former research [20]. The mass loadings were controlled to be 5.9 mg/cm^2 and the C rates were based on 1C=160 mA/g.

In the C rate experiment shown in Figure 3.7 (a), the Hexyl-ProDOT and PVDF coin cells exhibit a similar high specific capacity at low C rate, 168 mAh/g and 166 mAh/g at C/5 rate respectively. These values are close to the theoretical specific capacity of the NCA material. However, the Hexyl-ProDOT cell shows higher specific capacity retention than the PVDF cell does at 2C or higher rates. The Hexyl-ProDOT keeps a capacity of 111 mAh/g at 6C rate, while the PVDF shows a capacity less than 20 mAh/g at the same rate. Thus, the Hexyl-ProDOT significantly enhanced the capacity at high C-rates for NCA half-cells compared to that of the PVDF binder.

The Figure 3.7 (b) shows the long-term experiment for coin cells with these two different binders at a 2C rate for 200 cycles. In the first 120 cycles, both Hexyl-ProDOT and PVDF coin cells show a linear decrease in specific capacity and the difference between the degradation rates of these two groups can hardly be identified. However, severe decay can be observed with the PVDF coin cell after 120 cycles, while the Hexyl-ProDOT coin cell exhibits a similar degradation rate as that of the first 120 cycles. This result indicates that the Hexyl-ProDOT

shows better stability during the long-term cycling and provides enhanced capacity retention for the NCA half-cells.

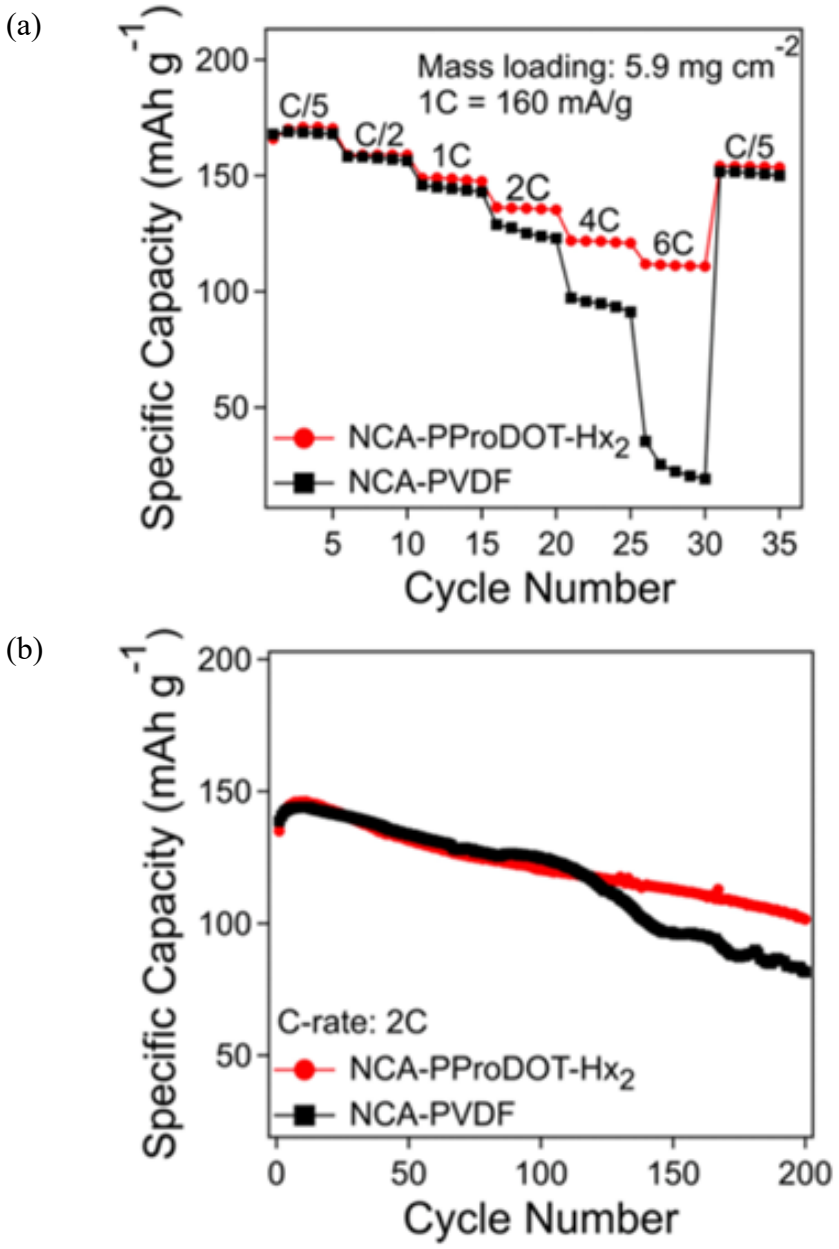

Figure 3.7 NCA-Li metal half-cell experiment data using Hexyl-ProDOT and PVDF as the NCA electrode binders at different current rates. (a) Rate capability of the NCA- Hexyl-

ProDOT and NCA-PVDF half-cell. (b) Long term stability of the NCA- Hexyl-ProDOT and NCA-PVDF half-cell at 2C current rate for 200 cycles [20].

Figure 3.8 represents the rate capability comparison between the NCA half-cells using different conductive binders, Hexyl-ProDOT and (75:25) (Hex:OE)-CoProDOT. The Hexyl-ProDOT half-cell sample in Figure (a) shows 160.2 mAh/g specific capacity at C/2 rate and it retains 70% of this value at the 6C rate. Although, capacity degradation exists, it occurs at a stable rate and at a relatively small amount compared to the C/2 rate performance. However, the CoProDOT sample shows much worse performance (Figure (b)). The total capacity of CoProDOT cell at C/2 only achieves 132.8 mAh/g, and it drops to 38.7% of this value at the 6C rate. The capacity decrease is particularly severe for experiments at higher than the 2C rate. It is also clear that the charging and discharging curves of the CoProDOT group are non-linear at 4C and 6C. The results indicate that CoProDOT coin cells not only exhibit lower capacity at all the tested C rates, but also exhibit poor performance at high C rate. The Hexyl-ProDOT coin cell shows both high capacity and good stability in the experiments. Although the oligoether (OE) side chain modified CoProDOT behaves similarly to the Hexyl-ProDOT in thin film experiments with pure polymer binders, the NCA half-cell with Hexyl-ProDOT binder shows much better performance than the cell with CoProDOT. Thus, the OE side chain changes how the binder interacts with the NCA active material and limits the properties of the NCA electrodes.

(a)

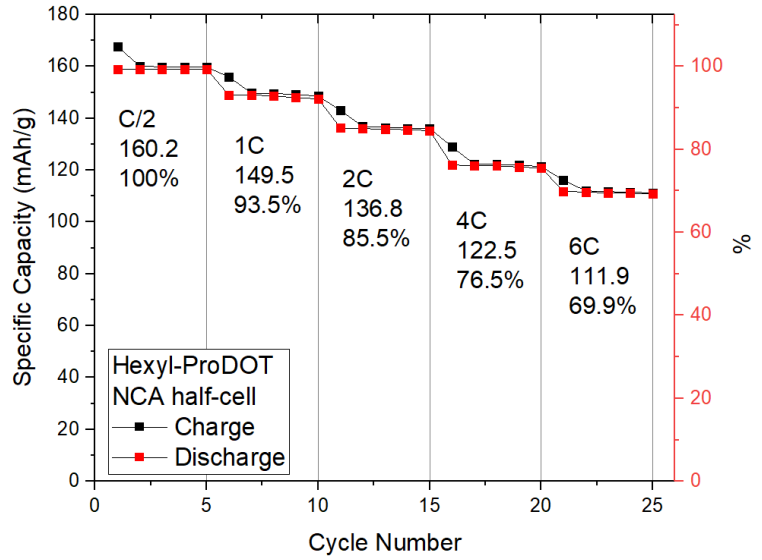
Specific Capacity (mAh/g)
%
Cycle Number
C/2
160.2
100%
1C
149.5
93.5%
2C
136.8
85.5%
4C
122.5
76.5%
6C
111.9
69.9%
Hexyl-ProDOT
NCA half-cell
Charge
Discharge

(b)

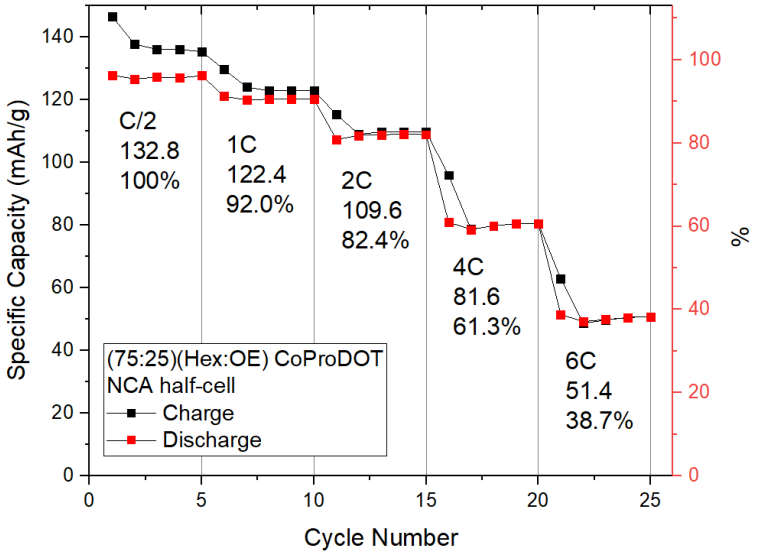
Specific Capacity (mAh/g)
%
Cycle Number
C/2
132.8
100%
1C
122.4
92.0%
2C
109.6
82.4%
4C
81.6
61.3%
6C
51.4
38.7%
(75:25)(Hex:OE) CoProDOT
NCA half-cell
Charge
Discharge

(c)

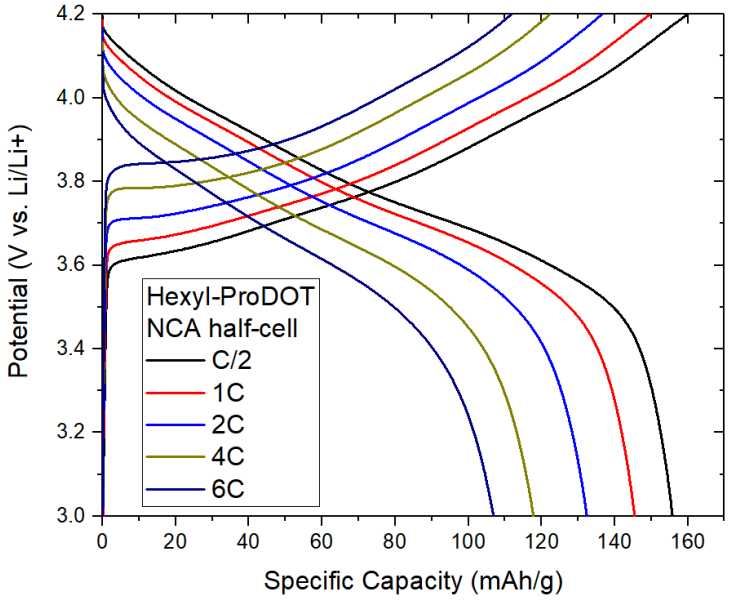
Potential (V vs. Li/Li+)
Specific Capacity (mAh/g)
Hexyl-ProDOT
NCA half-cell
C/2
1C
2C
4C
6C

(d)

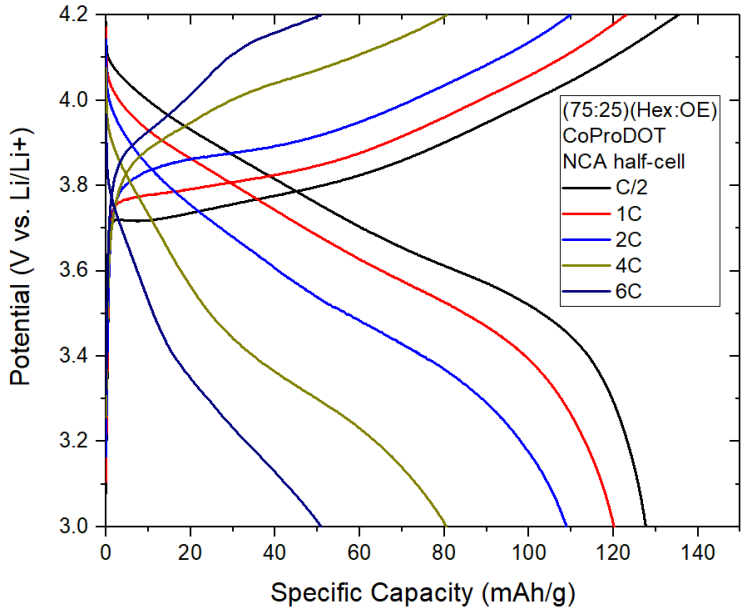

Figure 3.8 NCA-Li metal half-cell C rate experiment data with a potential window ranging from 3.0 to 4.2 V vs. Li/Li+ at different C rates, using Hexyl-ProDOT and (75:25) (Hex:OE)-CoProDOT as the NCA electrode binders respectively. (a) Rate capability of the NCA half-cell with Hexyl-ProDOT binder. (b) Rate capability of the NCA half-cell with (75:25) (Hex:OE)-CoProDOT binder. (c) Corresponding curves at 3rd cycle of each C rate for Hexyl-ProDOT cell. (d) Corresponding curves at 3rd cycle of each C rate for (75:25) (Hex:OE)-CoProDOT cell.

3.3 Results and discussion of full-cell experiments

In order to evaluate how the binder affects battery performance, three groups of polymer binder, Hexyl-ProDOT, (75:25) (Hex:OE)-CoProDOT and PVDF, are used with NCA cathodes in the fabrication of NCA-Nb_2O_5 full cells. The NCA cathode mass loadings are controlled to be 1 mg/cm^2 for all three groups, and the Nb_2O_5:NCA anode-cathode mass

loading ratio is balanced to be 8:7, based on the specific capacity difference (Nb_2O_5: 140 mAh/g, NCA: 160 mAh/g). The cell voltage range in CV experiments for the NCA-Nb_2O_5 full cells is selected to be 1.0~3.0V because the NCA stores charge in the 3.0~4.2 V vs. Li/Li+ range and Nb_2O_5 stores charge in the 1.2~2.2 V vs. Li/Li+ range.

Figure 3.9 shows the CV results for the NCA-Nb_2O_5 full cells. All three CV results show similar profiles due to the same NCA-Nb_2O_5 active materials. However, there are still differences in detail which can be detected for the differnent cathode binders. The Hexyl-ProDOT shows the highest current at each charging and discharging peak. The highest specific current reaches 273.7 mA/g at the 2.33 V charging peak when scanning at 0.5 mV/s. However, the specific currents are less than 200 mA/g under the same conditions for both the CoProDOT and PVDF cells. In addition, the reletively higher b value indicates that currents in the Hexyl-ProDOT cell are more surface controlled, which may contribute to more rapid electrochemical reactions. It can be also shown that both CoProDOT and PVDF current peaks shift more than 0.3 V, while the peak shifts in Hexyl-ProDOT are smaller than 0.1 V at the same time. The CV results support that Hexyl-ProDOT used as the binder in NCA cathode would enhance the battery performance at higher charging and discharing rates. According to these CV experiments, the full cell using Hexyl-ProDOT shows significant enhancement compared to the CoProDOT and PVDF groups, and that the CoProDOT group bahavior is almost the same as the PVDF group. The surface-controlled mechanism for Hexyl-ProDOT doping/dedoping

may contribute to rapid redox in the NCA cathode reaction, and contribute to the NCA-Nb_2O_5 full cell performance.

(a)

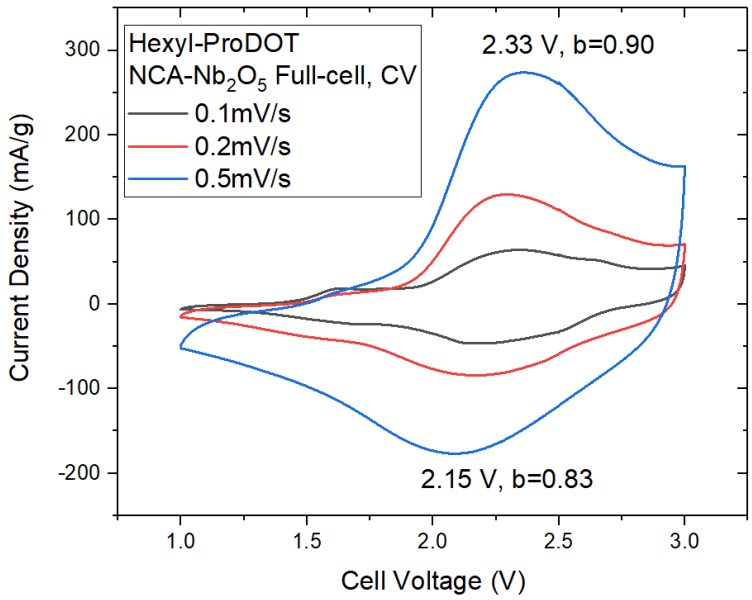

(b)

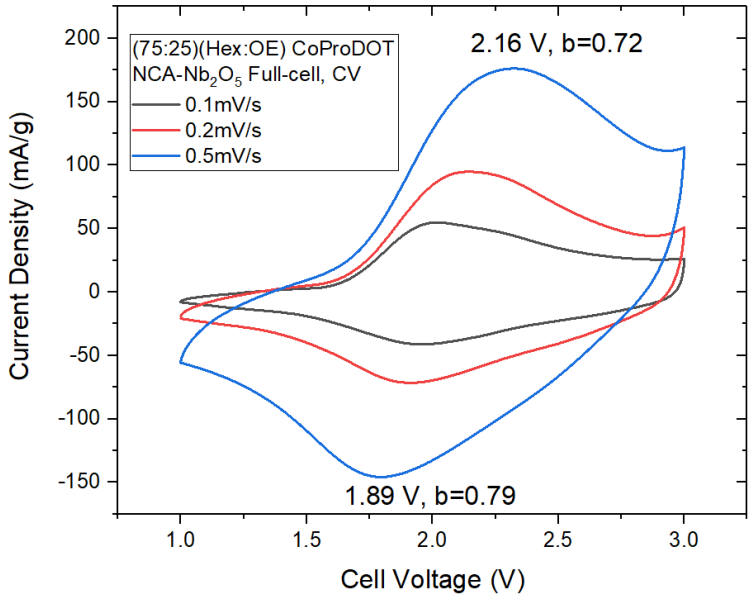

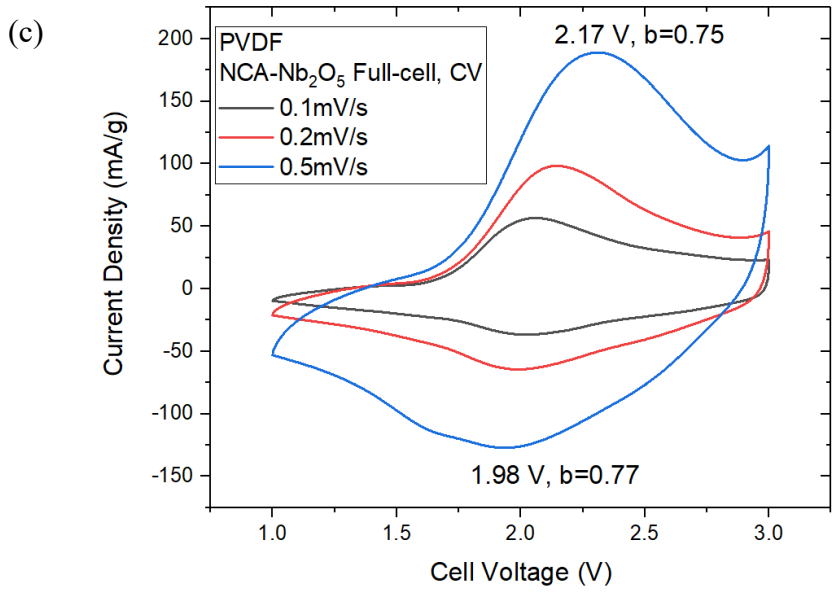

Figure 3.9 CV experiment data for NCA-Nb_2O_5 full cell at a potential window ranging from 1.0 to 3.0 V as a function of various sweep rates from 0.1 to 0.5 mV/s, using different binders for the NCA electrodes. (a) CV data using Hexyl-ProDOT as NCA cathode binder. (b) CV data using (75:25) (Hex:OE)-CoProDOT as NCA cathode binder. (c) CV data using PVDF as NCA cathode binder.

Figure 3.10 shows the C rate dependence on capacity for NCA-Nb_2O_5 full cells using different binders. Figure 3.10 (a) shows the comparision between the full cells using Hexyl-ProDOT and PVDF as the NCA cathode binder respectively. The performance of the Hexyl-ProDOT cell is significantly better than the PVDF cell. At the C/2 rate, the Hexyl-ProDOT cell achieves 123.5 mAh/g specific capacity while the PVDF cell can only achieve 96.4 mAh/g capacity. Addtionally, the Hexyl-ProDOT cell retains 75.1 mAh/g capacity at 2C (more than 60% ratio of the C/2 rate), while the capacity of the PVDF cell decreases to 27.5 mAh/g (almost 25% of the C/2 rate performance). Although a significant decrease in capacity can be observed

in the 5C rate experiment for Hexyl-ProDOT, it still shows higher capacity than that of the PVDF binder. Figure 3.10 (b) shows the comparision between full cells using CoProDOT and PVDF as the binders. However, there seem to be few differences between these two groups. The rate capability experiments establish that using Hexyl-ProDOT as the NCA cathode binder should strongly enhance battery performance at different charging and discharging rates.

(a)

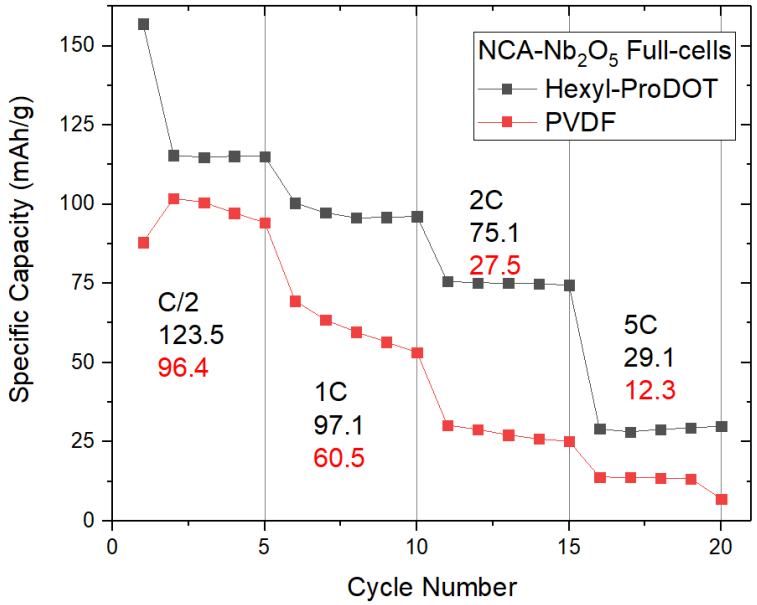

(b)

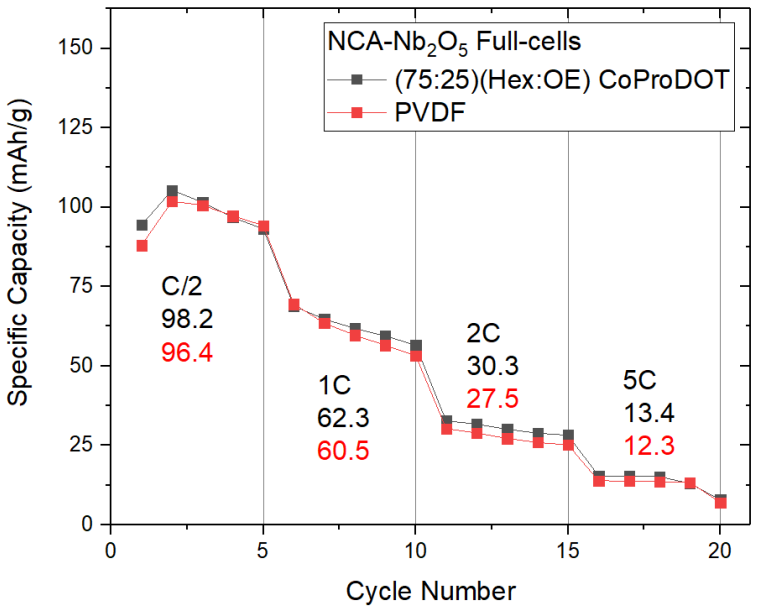

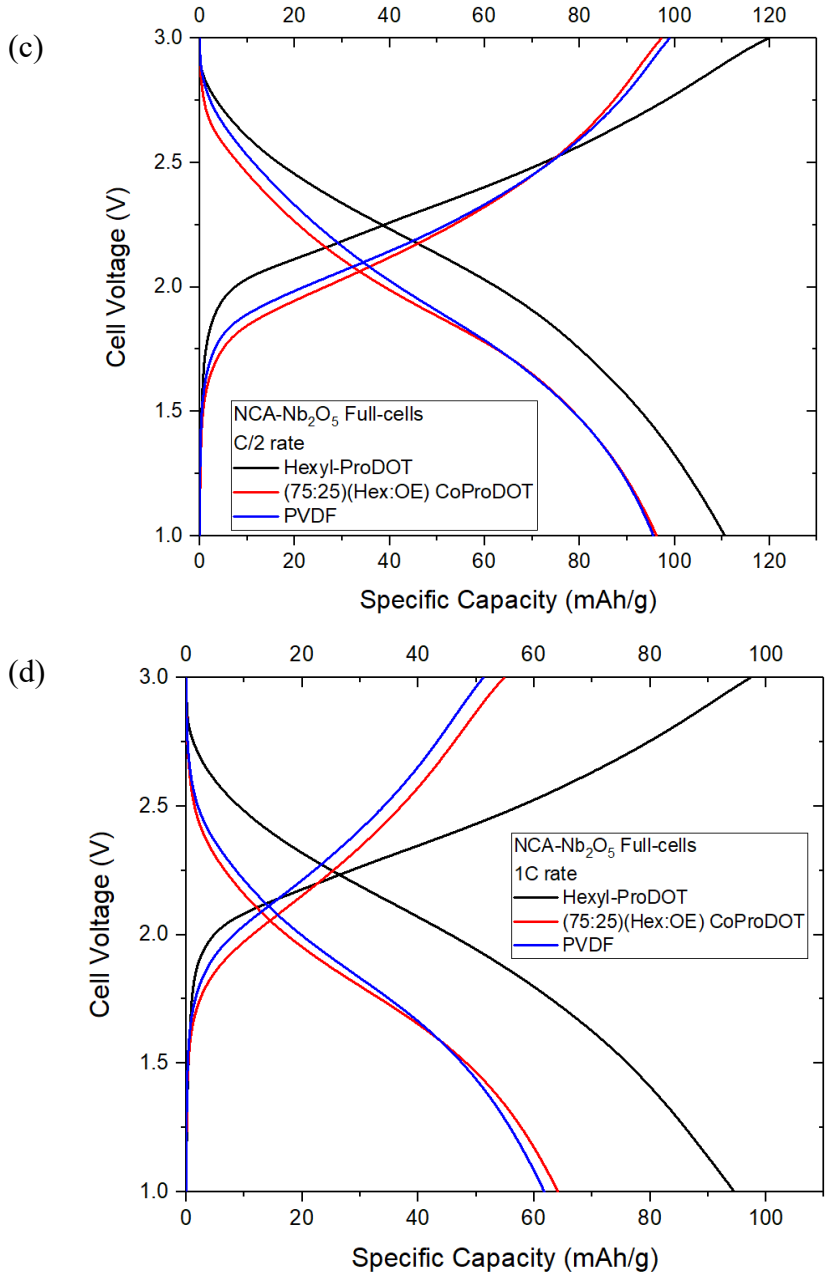

Figure 3.10 C rate experiment data for NCA-Nb_2O_5 full cell with a potential window ranging from 1.0 to 3.0 V at different C rates, using different binders for the NCA electrodes. (a) Rate capability comparison between full cells with Hexyl-ProDOT and PVDF. (b) Rate capability comparison between full cells with (75:25) (Hex:OE)-CoProDOT and PVDF. (c) Corresponding curves at 3rd cycle of C/2 rate experiments for all three cells. (d) Corresponding curves at 3rd cycle of 1C rate experiments for all three cells.

3.4 Summary

The Hexyl-ProDOT polymer binder was tested in thin film three-electrode cells, NCA-lithium half-cells and NCA-Nb_2O_5 full-cells with the goal of determining its performance as an electrode binder. The thin film three-electrode experiments indicate that the polymer has extremely high b value close to 1.0 resulting from a surface-controlled doping/dedoping mechanism. The surface-controlled process leads to rapid redox reactions and indicates Hexyl-ProDOT is a good candidate for being a conductive binder. Additionally, Hexyl-ProDOT can contribute to the capacity, although the amount is small. The NCA-Lithium half-cell experiments are able to characterize how the ploymer behaves in an actual battery electrode under cycling conditions and how it compares to the commonly used PVDF binder. The C rate experiments show that both Hexyl-ProDOT cell and PVDF cells possess capacities close to the theoratical value at 1C or lower C. At high C rate, however, the Hexyl-ProDOT cell performs much better than the PVDF cell, especially at 6C where Hexyl-ProDOT cell exhibits 111 mAh/g capacity while PVDF cell is less than 20 mAh/g. Moreover, under extended cycling (200 cycles) at the 2C rate, Hexyl-ProDOT shows stable capacity retention while the PVDF cell decays severely the 120^{th} cycle. In the NCA-Nb_2O_5 full-cell experiments which simulate how a practical battery works, the Hexyl-ProDOT maintains the outstanding performance shown in the half-cell experiments and exhibits much better performance compared to the full-cell with the PVDF binder. Taken together, the results of these experiments establish that

Hexyl-ProDOT leads to improved battery capacity and stability when used as the cathode binder.

The (75:25) (Hex:OE)-CoProDOT with the oligoether (OE) side chain modification was also investigated using analogous experiments to those with Hexyl-ProDOT. The thin film three-electrode experiments show that the CoProDOT possesses similar electrochemical properties as those of Hexyl-ProDOT, however, CoProDOT cannot achieve the same level of performance. Moreover, both the CoProDOT half-cell and full-cell fail to show significantly different performance compared to PVDF cells under the same experimental conditions. Because the NCA-CoProDOT electrodes fail in coin cell experiments, we propose that the NCA-binder properties changed due to the OE side chain modification, leading to the poor battery performance. These experiments show that (75:25) (Hex:OE)-CoProDOT does not offer any advantage as a cathode binder and does not lead to enhanced battery performance.

4. Performance of conductive polymer P(NDI2OD) as anode binder

4.1 Results and discussion of thin film experiment

The electrochemical performance of a potential anode binder, P(NDI2OD-T2), was investigated experimentally in three-electrode experiments. Figure 4.1 shows the CV results for P(NDI2OD-T2) thin film samples. From the Figure 4.1 (a), the CV curves of the P(NDI2OD-T2) thin films show two current peaks when charging, located at 2.38 V and 2.58 V respectively. The two charging peaks suggest the existence of two Li ion doping sites for the

P(NDI2OD-T2) polymer. In contrast, there is only one broadened discharge peak located at 2.23 V on the CV curve. In order to distinguish the exact positions of the discharge peaks corresponding to the two de-doping peaks, the CV curves shown in Figure 4.1 (b) were obtained over different voltage ranges. According to the results shown in Figure 4.1 (b), the one broad discharge peak can be treated as two overlapping peaks because only one charging peak can be detected when the discharge stops at 2.1 V, which is in the middle of the broad discharge peak.

The b value analysis results are labeled in Figure 4.1 (a). The first charging peak shows a high b value of 0.89 at 2.38 V, while the second charging peak shows a significantly lower b value of 0.66 at 2.58 V. The discharge peak exhibits a b value 0.56 at 2.23 V. The different b values indicate that the Li ion doping/dedoping mechanism varies during the charging and discharging procedure due to the different sites in the polymer structure.

(a)

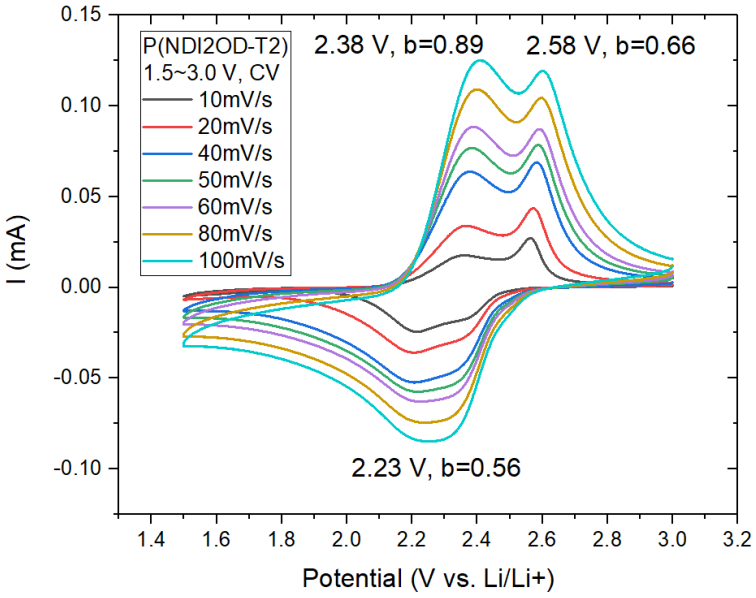

(b)

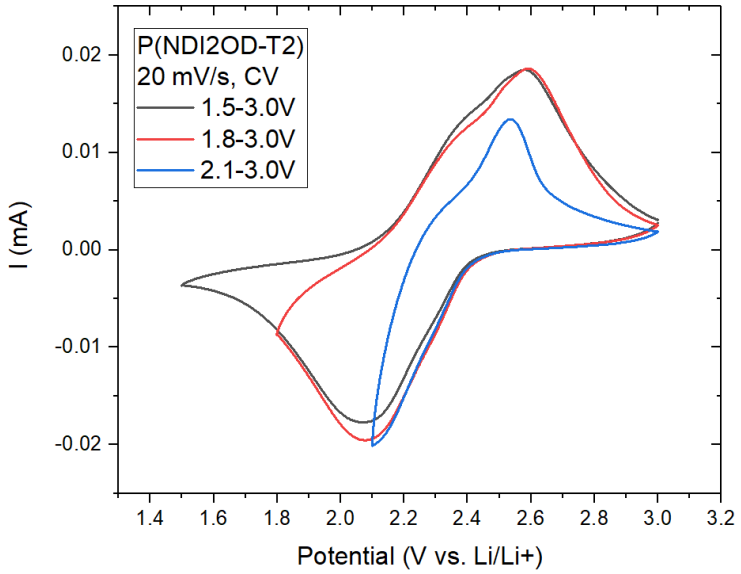

Figure 4.1 CV experiment data for P(NDI2OD-T2) thin film. (a) CV curves for P(NDI2OD-T2) thin film cycled with a potential window ranging from 1.5 to 3.0 V vs. Li/Li+ as a function of various sweep rates from 10 to 100 mV/s. (b). CV curves for P(NDI2OD-T2) thin film cycled at a sweep rate of 20 mV/s as various potential windows.

In order to improve the performance of the P(NDI2OD-T2) polymer, the P(NDI2OD-T2) polymer was modified with an additive agent (20% ratio) in the polymer main chain. The thin film CV results for the modified polymer P(NDI2OD-T2) 20% T-6-T are shown in Figure 4.2. The CV performance for the modified binder is similar to that of the P(NDI2OD-T2) sample. Both polymers show one broad discharge peak and two charging peaks, and the one broad discharge peak can be treated as two overlapping peaks. The difference introduced by the additive agent is in the b value analysis, as the b value for the first charging peak of the modified polymer is 0.63 at 2.31 V while the corresponding result for P(NDI2OD-T2) is 0.89 at 2.38 V.

This result indicates that the transport mechanism for the modified binder has become more diffusion-controlled.

Figure 4.2 (c) and (d) display the CV results for the P(NDI2OD-Se) thin film sample, which is modified with the P(NDI2OD-T2) monomers. The characteristic at high sweep rates and relatively high current value at the end of the discharge (1.5 V) suggests that the polymer has poor stability at fast charge/discharge rates and/or at low potentials. This result does not meet the requirement for the conductive polymer binder to be used for high-rate and low-voltage anodes. For this reason, only the P(NDI2OD-T2) polymer will be tested in the following experiments.

(a)

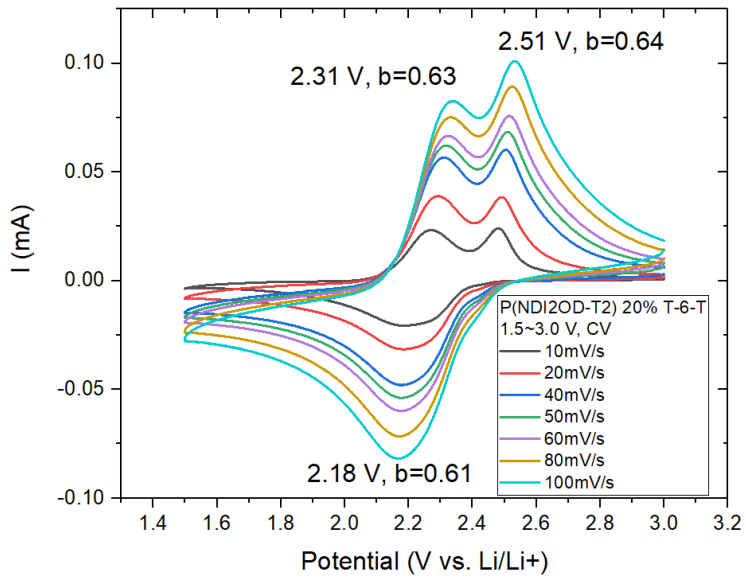

(b)

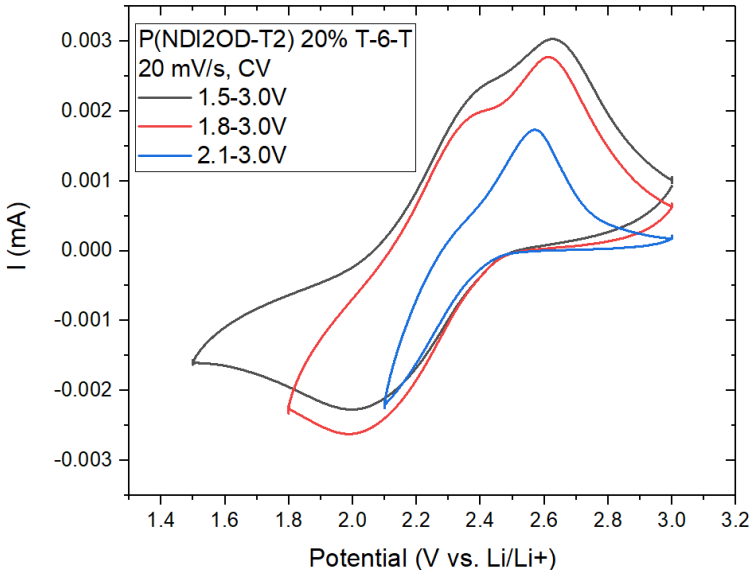
P(NDI2OD-T2) 20% T-6-T
20 mV/s, CV
1.5-3.0V
1.8-3.0V
2.1-3.0V
I (mA)
Potential (V vs. Li/Li+)

(c)

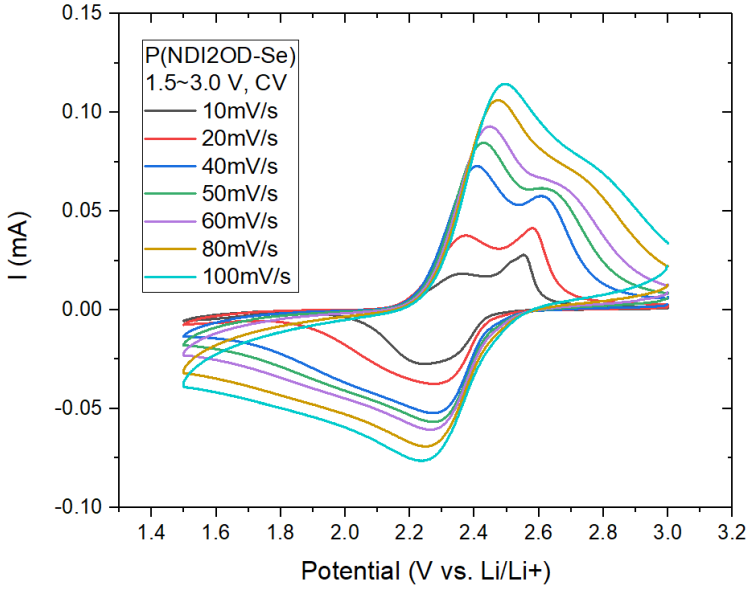
P(NDI2OD-Se)
1.5~3.0 V, CV
10mV/s
20mV/s
40mV/s
50mV/s
60mV/s
80mV/s
100mV/s
I (mA)
Potential (V vs. Li/Li+)

(d)

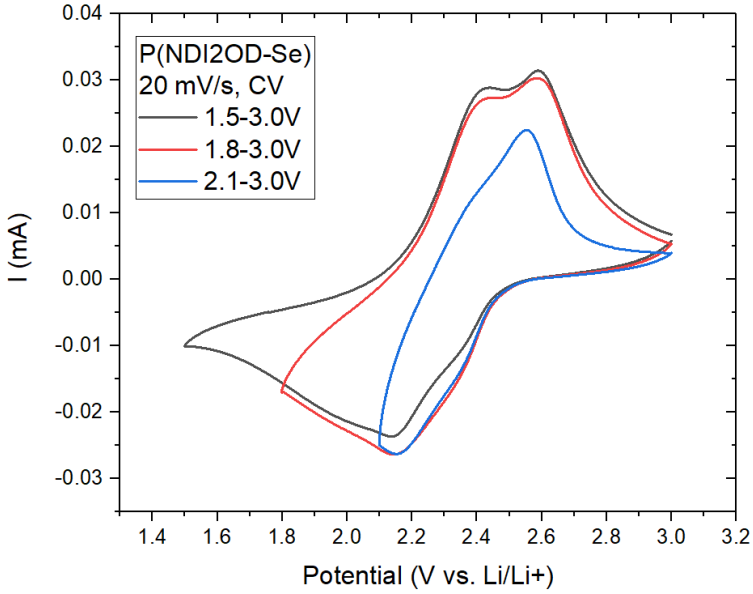
P(NDI2OD-Se)
20 mV/s, CV
1.5-3.0V
1.8-3.0V
2.1-3.0V
I (mA)
Potential (V vs. Li/Li+)

Figure 4.2 CV experiment data for P(NDI2OD-T2) 20% T-6-T and P(NDI2OD-Se) thin film. (a) CV curves for T-6-T sample cycled with a potential window ranging from 1.5 to 3.0 V vs. Li/Li+ as a function of various sweep rates from 10 to 100 mV/s. (b). CV curves for T-6-T sample cycled at a sweep rate of 20 mV/s as various potential windows. (c) CV curves for Se sample cycled with a potential window ranging from 1.5 to 3.0 V vs. Li/Li+ as a function of various sweep rates from 10 to 100 mV/s. (d). CV curves for Se sample cycled at a sweep rate of 20 mV/s as various potential windows.

The stability experiments for the P(NDI2OD-T2) thin film are shown in the Figure 4.3. Two P(NDI2OD-T2) thin film samples are cycled at the 10 mV/s rate but over different voltage ranges (1.3~3.0 V and 1.5~3.0 V) for 20 cycles. The capacity degradation curves are shown in Figure 4.3 (a). The similar capacity gaps between charging and discharging procedures can be found for both 1.5~3.0 V range and 1.3~3.0 V range. These experimental results indicate that the gap for the 1.3~3.0 V range is larger than that for 1.5~3.0 V. As the number of cycles increases, the gap for the 1.5~3.0 V range gradually shrinks, while the gap for the 1.3~3.0 V range remains basically unchanged. The CV curves for the 3rd cycles are recorded in Figure 4.3 (b). This figure shows that there is a significant current peak in the 1.3~3.0 V CV curve, which is located at 1.3 V where the discharge ends. The current increase is indicative of an irreversible reaction which results from the poor stability of the polymer at voltages lower than 1.5 V. In comparison, the smaller capacity gap for the 1.5~3.0 V range suggests that the irreversible reactions tend to be avoided, while the irreversible reaction remains throughout the

entire 20 CV cycles for the 1.3~3.0 V range. This experiment establishes that the P(NDI2OD-T2) polymer is relatively stable in the 1.5~3.0 V range, but does not perform well in the 1.3~3.0V range. The poor stability at low potential will not be beneficial for use with anode materials such as LTO, whose electrochemical reactions mainly occur at 1.3~1.9 V vs. Li/Li+.

(a)

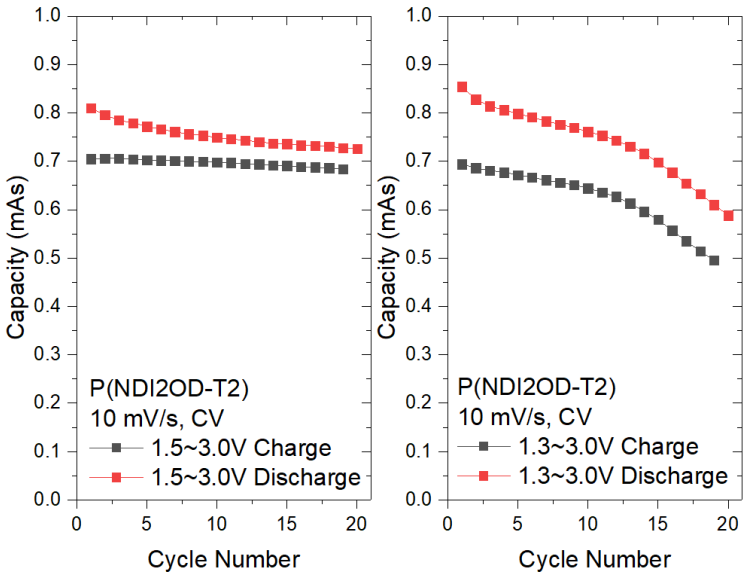

(b)

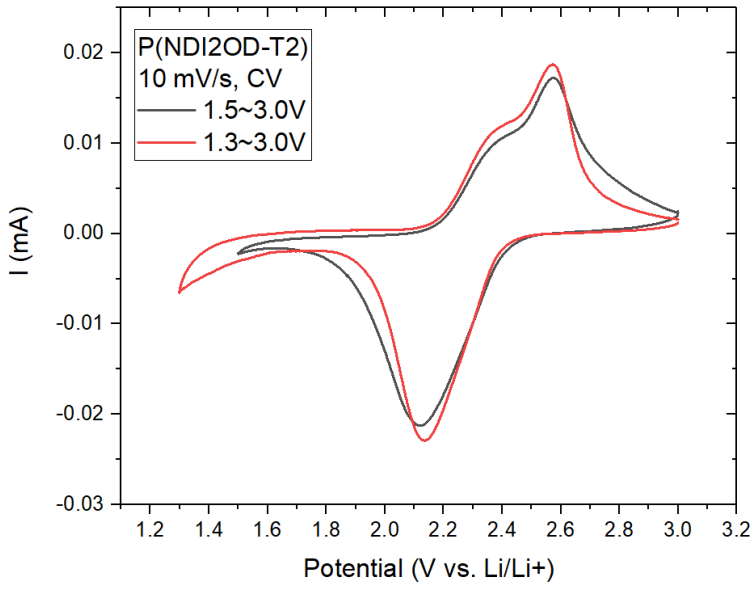

Figure 4.3 Stability experiments for P(NDI2OD-T2) thin film. (a) Capacity degradation during the CV over different voltage ranges at 10 mV/s sweep rate. (b) CV curves for P(NDI2OD-T2) thin film at different voltage ranges at the same 10 mV/s sweep rate.

4.2 Results and discussion of half-cell experiment

Figure 4.4 shows the CV results for LTO half-cells using P(NDI2OD-T2) or PVDF as anode binders. The CV curves for the two different binders share similar characteristics with one pair of charging and discharging peaks related to the 90% mass loading of LTO active material. In the CV curve of P(NDI2OD-T2) cell, the weak charge/discharge peaks can be detected in the range of 2.0~2.7 V. These current peaks match the P(NDI2OD-T2) thin film CV experimental results, which indicate that P(NDI2OD-T2) contributes to the battery capacity, although it is very small. Compared to the PVDF cells, the CV curves of P(NDI2OD-T2) cells show a larger peak shift of 0.1 V and a higher current at 1.3 V representing an irreversible reaction, which is similar to the results of the thin film experiments in Figure 4.3 (b). This result suggests that even with a binder content of only 4%, the poor stability of the P(NDI2OD-T2) binder may have a significant impact on the LTO half-cell performance.

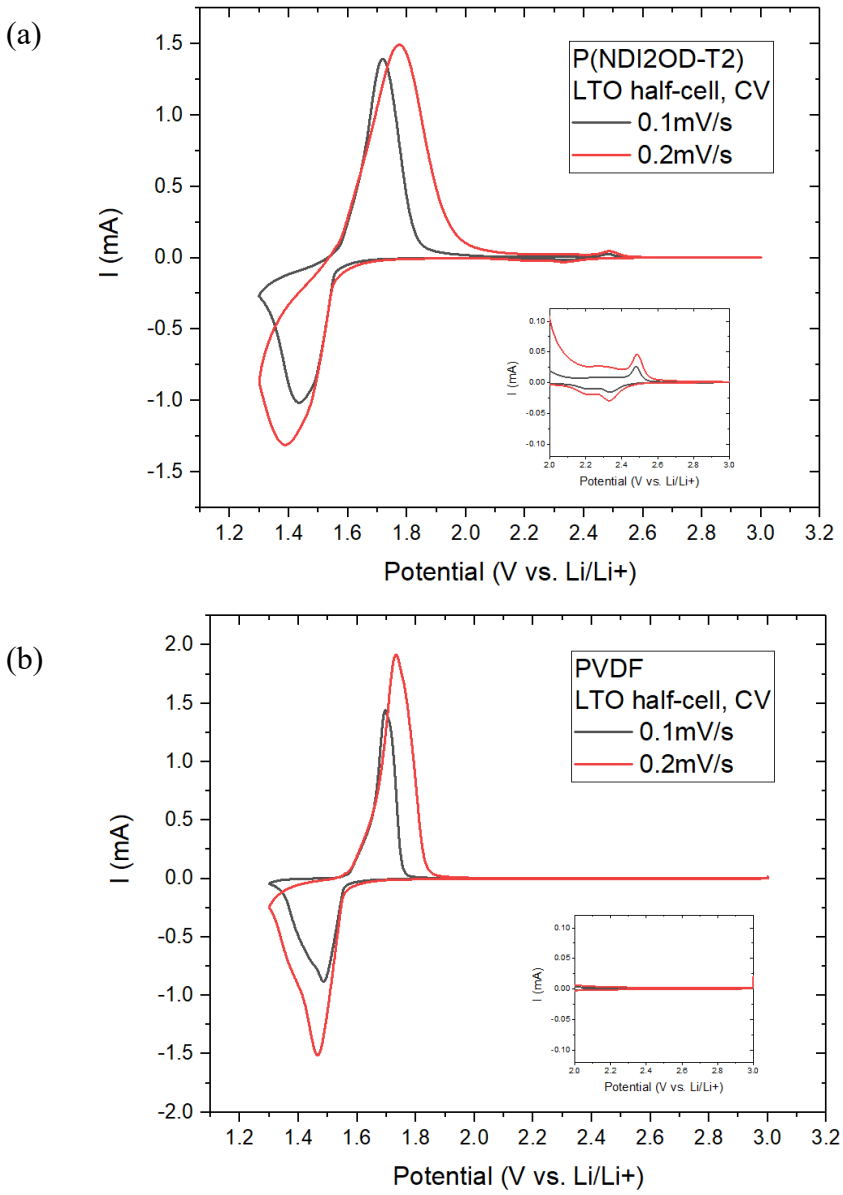

Figure 4.4 CV experiments data for LTO-Li metal half-cell with a potential window ranging from 1.3 to 3.0 V vs. Li/Li+ at different sweep rates, using P(NDI2OD-T2) and PVDF as the LTO electrode binders respectively. (a) P(NDI2OD-T2) half-cell experiment data. (b) PVDF half-cell experiment data.

The C rate experiments for the LTO half-cell with using P(NDI2OD-T2) or PVDF as anode binders are shown in Figure 4.5. The P(NDI2OD-T2) cell and PVDF cell show 175.6 mAh/g and 172.2 mAh/g specific capacity at the C/5 slow rate respectively, which are close to the theoretical condition. The capacity gaps between the two samples become larger with increasing current, and the capacity degradation for P(NDI2OD-T2) cell is much more severe than that for the PVDF cell. The P(NDI2OD-T2) cell retains 47% capacity at the 6C rate while there 64% capacity remains in the PVDF cell. In addition, there is also a capacity difference between the first 2C cycles (16^{th}~20^{th} cycles) and the final 2C cycles (31^{st}~35^{th} cycles). The difference exists in both P(NDI2OD-T2) cell and PVDF cell, although it is relatively more severe in the P(NDI2OD-T2) cell. These capacity-rate experiments which compare the LTO-P(NDI2OD-T2) half-cell and LTO-PVDF half-cell indicate that the P(NDI2OD-T2) anode binder limits battery performance, especially under high charging and discharging rate conditions.

(a)

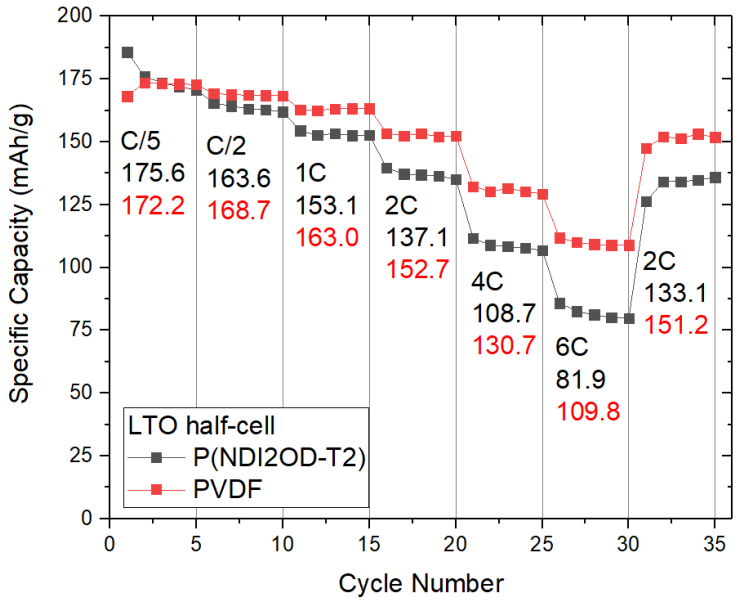

(b)

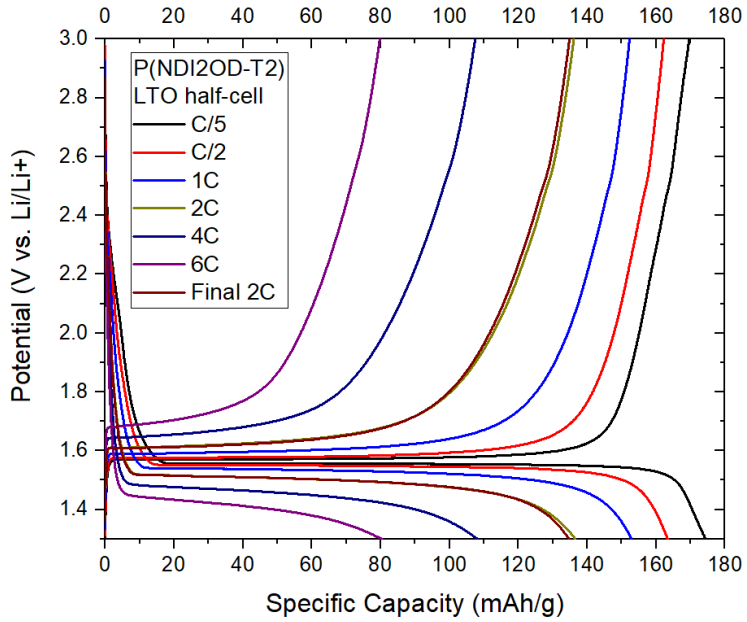

(c)

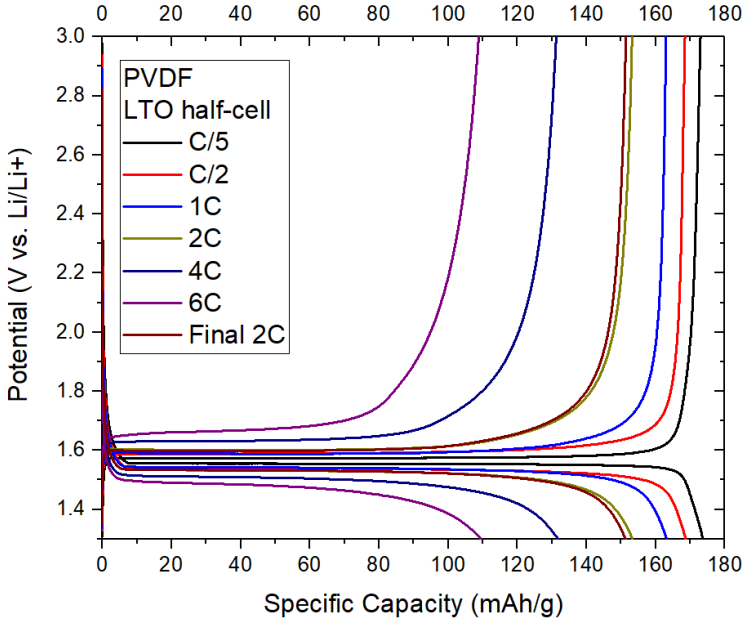

Figure 4.5 C rate experiment data for LTO-Li metal half-cells with a potential window ranging from 1.5 to 3.0 V vs. Li/Li+ at different C rates, using P(NDI2OD-T2) and PVDF as the LTO electrode binders respectively. (a) Rate capability comparison between half-cells with P(NDI2OD-T2) and PVDF. (b) Corresponding curves at 3rd cycle of each C rate cycles for P(NDI2OD-T2) cell. (b) Corresponding curves at 3rd cycle of each C rate cycles for PVDF cell.

4.3 Summary

The P(NDI2OD-T2) polymer is investigated for its performance as an anode binder along with two modified systems, P(NDI2OD-T2) 20% T-6-T and P(NDI2OD-Se). According to the thin film three-electrode experiments, the P(NDI2OD-T2) polymer shows lithium capacity and conductivity at the 1.5~3.0 V range while the b value analysis indicates that both surface-controlled and diffusion-controlled processes exist during the cycling. The experiments also suggest that there are stability problems when cycling the P(NDI2OD-T2) thin film sample at the lower voltage range of 1.3~3.0 V, which is the regime required for commonly used anode materials such as LTO. As for the modified polymers, the P(NDI2OD-T2) 20% T-6-T is mainly diffusion-controlled when cycled in the 1.5~3.0 V range while the P(NDI2OD-Se) shows poor stability in the same voltage range. For this reason, only the P(NDI2OD-T2) polymer was tested in half-cell experiments. Compared to the LTO half-cell using PVDF as the anode binder, the P(NDI2OD-T2) half-cell exhibits an irreversible reaction at 1.3 V and severe capacity loss occurs when cycling at 1C or higher rate. At 6C, the P(NDI2OD-T2) half-cell can only keep 81.9 mAh/g specific capacity while 109.8 mAh/g is retained in PVDF half-cell. The present experiments prove that P(NDI2OD-T2) limits the performance of the LTO electrode due to its poor stability and diffusion-controlled doping/dedoping mechanism. These results indicate that there is still a need to develop new anode binder materials with good stability at 1.0 V or lower voltage and surface-controlled doping/dedoping processes for high-rate performance.

5. Conclusion and outlook

In this thesis, two conjugated polymer families, ProDOT family and P(NDI2OD-T2) family, are evaluated for their feasibility in being used for the LIB binder. The thin film experiments, half-cell experiments and full-cell experiments are designed and carried out on both of the polymers in order to investigate their binder performance at different levels of operation. The thin film experiments with pure polymer tested in the three-electrode system provide information regarding the electrochemical properties and redox behavior of the polymers under conditions where there is no contribution from other binders or additives. The half-cell experiments reveal how the working electrodes fabricated using the sample polymer and the selected active material behave under typical battery operating conditions. In these studies, the Li metal counter electrode does not affect the energy density or power density of the electrode. The full-cell experiments are conducted using commonly studied active materials as both cathode and anode. These studies provide an understanding of how the polymer binder influences practical battery systems. Based on the analysis and discussion of the experimental results, the performance of the ProDOT and P(NDI2OD-T2) families can be assessed.

The Hexyl-ProDOT shows good cycling stability in the 3.0~4.2 V voltage window and a surface-controlled electrochemical doping/dedoping mechanism in the thin film three-electrode cell experiments. These results suggest that Hexyl-ProDOT is a potential binder for improving the rate performance of the NCA cathode. Compared to the NCA-PVDF half-cell experiments, the Hexyl-ProDOT cells offer enhanced battery performance, especially at 4C

and 6C rates, along with higher capacity retention in long-term cycling experiments. In the NCA-Nb_2O_5 full cell experiments, cells with the Hexyl-ProDOT binder exhibit advantages in rate capability over the PVDF binder cells at all cycling rates. The (75:25) (Hex:OE)-CoProDOT with the oligoether (OE) side chain modification behaves similarly in the thin film experiments as that of Hexyl-ProDOT. However, the CoProDOT fails to show any performance enhancement in the half-cell or full-cell experiments when compared to PVDF. In summary, these experiments indicate that the Hexyl-ProDOT cathode binder is able to improve the LIB rate capability and cycling performance due to the mixed ionic/electronic conductivity and surface-controlled reaction mechanism. The CoProDOT cathode binder does not offer any the improvement.

The P(NDI2OD-T2) polymer shows mixed surface-controlled and diffusion-controlled doping/dedoping mechanism in the thin film three-electrode cell experiments. Its stability at low voltage is relatively poor at 1.3 V but is acceptable at 1.5 V. In half-cell experiments using the P(NDI2OD-T2) polymer binder with the LTO anode material, the rate performance is significantly reduced compared to electrodes fabricated with the PVDF binder. Additionally, two modified polymers, P(NDI2OD-T2) 20% T-6-T and P(NDI2OD-Se), show even worse stability and the less desirable diffusion-controlled kinetics in thin film experiments. Thus, the P(NDI2OD-T2) is not feasible as the LIB anode binder, unless the poor stability at low voltage and the diffusion-controlled doping/dedoping process can be modified.

Although this thesis provides preliminary results regarding the use of ProDOT and P(NDI2OD-T2) polymers as conductive binders, there are still many issues which require further research.

For the ProDOT family, there are still modification, beyond Hexyl-ProDOT, which can be tried in order to improve such features as increasing the potential window to higher voltage or suppressing irreversible side-reactions. For practical applications for the Hexyl-ProDOT, there needs to be greater understanding of how binder operating conditions switch from experimental cells to commercialized cells. The conditions of higher electrode mass loading and longer-term cycling in the practical battery will challenge different aspects of the binder materials, including the mechanical strength, electrolyte swelling rate, stability and conductivity. Thus, there is a need to continue research on both the modification of ProDOT materials and its extension into cell actual manufacturing.

As for the P(NDI2OD-T2) family, it is necessary to discover the internal causes which lead to the poor stability at lower voltage before investigating other binder properties. More conductive polymers with low voltage stability need to be identified and investigated.

Compared to the traditional binder, PVDF, used in the LIBs, the conductive polymers not only promise better adhesion and mechanical strength, but also greater ionic/electronic conductivity which improves the battery rate capability and cyclic stability. Although some new problems are introduced into the system, such as lower binder stability in the conductive

binders, those problems can be solved or mitigated through chemical modification. Additionally, the use of conductive binder could possibly reduce or even replace the use of conductive agents in the electrodes, which simplifies the fabrication of commercial battery products. For these reasons, the development of multi-functional binders should be recognized as a potential direction for future battery research and development.

6. Reference

[1] White House. (2021). Building Resilient Supply Chains, Revitalizing American Manufacturing, and Fostering Broad-based Growth: 100-Day Reviews under Executive Order 14017. A Report by The White House.

[2] Etacheri, V., Marom, R., Elazari, R., Salitra, G., & Aurbach, D. (2011). Challenges in the development of advanced Li-ion batteries: a review. Energy & Environmental Science, 4(9), 3243-3262.

[3] Whittingham, M. S. (1976). Electrical energy storage and intercalation chemistry. Science, 192(4244), 1126-1127.

[4] Mizushima, K. J. P. C., Jones, P. C., Wiseman, P. J., & Goodenough, J. B. (1980). Li_xCoO_2 ($0< x<-1$): A new cathode material for batteries of high energy density. Materials Research Bulletin, 15(6), 783-789.

[5] Dunn, B., Kamath, H., & Tarascon, J. M. (2011). Electrical energy storage for the grid: a battery of choices. Science, 334(6058), 928-935.

[6] Manthiram, A. (2020). A reflection on lithium-ion battery cathode chemistry. Nature communications, 11(1), 1-9.

[7] Yuan, L. X., Wang, Z. H., Zhang, W. X., Hu, X. L., Chen, J. T., Huang, Y. H., & Goodenough, J. B. (2011). Development and challenges of $LiFePO_4$ cathode material for lithium-ion batteries. Energy & Environmental Science, 4(2), 269-284.

[8] Andersson, A. M., Abraham, D. P., Haasch, R., MacLaren, S., Liu, J., & Amine, K. (2002). Surface characterization of electrodes from high power lithium-ion batteries. Journal of The Electrochemical Society, 149(10), A1358.

[9] Bak, S. M., Nam, K. W., Chang, W., Yu, X., Hu, E., Hwang, S., ... & Yang, X. Q. (2013). Correlating structural changes and gas evolution during the thermal decomposition of charged $Li_xNi_{0.8}Co_{0.15}Al_{0.05}O_2$ cathode materials. Chemistry of Materials, 25(3), 337-351.

[10] Aravindan, V., Lee, Y. S., & Madhavi, S. (2015). Research progress on negative electrodes for practical Li‐ion batteries: beyond carbonaceous anodes. Advanced Energy Materials, 5(13), 1402225.

[11] Kong, L., Cao, X., Wang, J., Qiao, W., Ling, L., & Long, D. (2016). Revisiting Li+ intercalation into various crystalline phases of Nb_2O_5 anchored on graphene sheets as pseudocapacitive electrodes. Journal of Power Sources, 309, 42-49.

[12] Griffith, K. J., Forse, A. C., Griffin, J. M., & Grey, C. P. (2016). High-rate intercalation without nanostructuring in metastable Nb_2O_5 bronze phases. Journal of the American Chemical Society, 138(28), 8888-8899.

[13] Yoo, M., Frank, C. W., Mori, S., & Yamaguchi, S. (2003). Effect of poly (vinylidene fluoride) binder crystallinity and graphite structure on the mechanical strength of the composite anode in a lithium ion battery. Polymer, 44(15), 4197-4204.

[14] McDowell, M. T., Lee, S. W., Nix, W. D., & Cui, Y. (2013). 25th anniversary article: understanding the lithiation of silicon and other alloying anodes for lithium - ion batteries. Advanced Materials, 25(36), 4966-4985.

[15] Zuo, X., Zhu, J., Müller-Buschbaum, P., & Cheng, Y. J. (2017). Silicon based lithium-ion battery anodes: A chronicle perspective review. Nano Energy, 31, 113-143.

[16] Sun, Y., Liu, N., & Cui, Y. (2016). Promises and challenges of nanomaterials for lithium-based rechargeable batteries. Nature Energy, 1(7), 1-12.

[17] Lopez, J., Mackanic, D. G., Cui, Y., & Bao, Z. (2019). Designing polymers for advanced battery chemistries. Nature Reviews Materials, 4(5), 312-330.

[18] Bounioux, C., Díaz-Chao, P., Campoy-Quiles, M., Martín-González, M. S., Goni, A. R., Yerushalmi-Rozen, R., & Müller, C. (2013). Thermoelectric composites of poly (3-hexylthiophene) and carbon nanotubes with a large power factor. Energy & Environmental Science, 6(3), 918-925.

[19] Lai, C. H., Ashby, D. S., Lin, T. C., Lau, J., Dawson, A., Tolbert, S. H., & Dunn, B. S. (2018). Application of poly (3-hexylthiophene-2, 5-diyl) as a protective coating for high rate cathode materials. Chemistry of Materials, 30(8), 2589-2599.

[20] Das, P., Zayat, B., Wei, Q., Salamat, C. Z., Magdău, I. B., Elizalde-Segovia, R., ... & Thompson, B. C. (2020). Dihexyl-substituted poly (3, 4-propylenedioxythiophene) as a dual ionic and electronic conductive cathode binder for lithium-ion batteries. Chemistry of Materials, 32(21), 9176-9189.

[21] Fu, Z., Feng, H. L., Xiang, X. D., Rao, M. M., Wu, W., Luo, J. C., ... & Li, W. S. (2014). A novel polymer composite as cathode binder of lithium ion batteries with improved rate capability and cyclic stability. Journal of Power Sources, 261, 170-174.

[22] Yabuuchi, N., Kinoshita, Y., Misaki, K., Matsuyama, T., & Komaba, S. (2015). Electrochemical properties of $LiCoO_2$ electrodes with latex binders on high-voltage exposure. Journal of the electrochemical society, 162(4), A538.

[23] Gao, S., Su, Y., Bao, L., Li, N., Chen, L., Zheng, Y., ... & Wu, F. (2015). High-performance $LiFePO_4$/C electrode with polytetrafluoroethylene as an aqueous-based binder. Journal of Power Sources, 298, 292-298.

[24] Qiu, L., Shao, Z., Wang, W., Wang, F., Wang, J., Wang, D., & Wang, Y. (2014). Enhanced Cyclability of C/Lithium Iron Phosphate Cathodes with a Novel water-soluble lithium-ion binder. Electrochimica Acta, 145, 11-18.

[25] Chong, J., Xun, S., Zheng, H., Song, X., Liu, G., Ridgway, P., ... & Battaglia, V. S. (2011). A comparative study of polyacrylic acid and poly (vinylidene difluoride) binders for spherical natural graphite/$LiFePO_4$ electrodes and cells. Journal of power sources, 196(18), 7707-7714.

[26] Ling, M., Qiu, J., Li, S., Yan, C., Kiefel, M. J., Liu, G., & Zhang, S. (2015). Multifunctional SA-PProDOT binder for lithium ion batteries. Nano letters, 15(7), 4440-4447.

[27] Pham, H. Q., Lee, J., Jung, H. M., & Song, S. W. (2019). Non-flammable $LiNi_{0.8}Co_{0.1}Mn_{0.1}O_2$ cathode via functional binder; stabilizing high-voltage interface and performance for safer and high-energy lithium rechargeable batteries. Electrochimica Acta, 317, 711-721.

[28] Chou, S. L., Wang, J. Z., Liu, H. K., & Dou, S. X. (2011). Rapid synthesis of $Li_4Ti_5O_{12}$ microspheres as anode materials and its binder effect for lithium-ion battery. The Journal of Physical Chemistry C, 115(32), 16220-16227.

[29] Nordh, T., Jeschull, F., Younesi, R., Koçak, T., Tengstedt, C., Edström, K., & Brandell, D. (2017). Different shades of $Li_4Ti_5O_{12}$ composites: The impact of the binder on interface layer formation. ChemElectroChem, 4(10), 2683-2692.

[30] Yen, J. P., Lee, C. M., Wu, T. L., Wu, H. C., Su, C. Y., Wu, N. L., & Hong, J. L. (2012). Enhanced high-temperature cycle-life of mesophase graphite anode with styrene–butadiene rubber/carboxymethyl cellulose binder. ECS Electrochemistry Letters, 1(6), A80.

[31] Chen, H., Ling, M., Hencz, L., Ling, H. Y., Li, G., Lin, Z., ... & Zhang, S. (2018). Exploring chemical, mechanical, and electrical functionalities of binders for advanced energy-storage devices. Chemical reviews, 118(18), 8936-8982.

[32] Wang, Y., Zhang, L., Qu, Q., Zhang, J., & Zheng, H. (2016). Tailoring the interplay between ternary composite binder and graphite anodes toward high-rate and long-life Li-ion batteries. Electrochimica Acta, 191, 70-80.

[33] Zou, F., & Manthiram, A. (2020). A review of the design of advanced binders for high‐performance batteries. Advanced Energy Materials, 10(45), 2002508.

[34] Chen, Z., Zheng, Y., Yan, H., & Facchetti, A. (2009). Naphthalenedicarboximide-vs perylenedicarboximide-based copolymers. Synthesis and semiconducting properties in

bottom-gate n-channel organic transistors. Journal of the American Chemical Society, 131(1), 8-9.

[35] Trefz, D., Ruff, A., Tkachov, R., Wieland, M., Goll, M., Kiriy, A., & Ludwigs, S. (2015). Electrochemical investigations of the n-type semiconducting polymer P (NDI2OD-T2) and its monomer: new insights in the reduction behavior. The Journal of Physical Chemistry C, 119(40), 22760-22771.

[36] Zayat, B., Das, P., Thompson, B. C., & Narayan, S. R. (2021). In situ measurement of ionic and electronic conductivities of conductive polymers as a function of electrochemical doping in battery electrolytes. The Journal of Physical Chemistry C, 125(14), 7533-7541.